

Information Geometric Aspects of Probability Paths with Minimum Entropy Production for Quantum State Evolution

Steven Gassner¹, Carlo Cafaro¹, Sean A. Ali², Paul M. Alsing³

¹*SUNY Polytechnic Institute, 12203 Albany, New York, USA*

²*Albany College of Pharmacy and Health Sciences, 12208 Albany, New York, USA and*

³*Air Force Research Laboratory, Information Directorate, 13441 Rome, New York, USA*

We present an information geometric analysis of both entropic speeds and entropy production rates arising from geodesic evolution on manifolds parametrized by pure quantum states. In particular, we employ pure states that emerge as outputs of suitably chosen $\mathfrak{su}(2; \mathbb{C})$ time-dependent Hamiltonian operators that characterize analog quantum search algorithms of specific types. The $\mathfrak{su}(2; \mathbb{C})$ Hamiltonian models under consideration are specified by external time-dependent magnetic fields within which spin-1/2 test particles are immersed. The positive definite Riemannian metrization of the parameter manifold is furnished by the Fisher information function. The Fisher information function is evaluated along parametrized squared probability amplitudes obtained from the temporal evolution of these spin-1/2 test particles. A minimum action approach is then utilized to induce the transfer of the quantum system from its initial state to its final state on the parameter manifold over a finite temporal interval. We demonstrate in an explicit manner that the minimal (that is, optimum) path corresponds to the shortest (that is, geodesic) path between the initial and final states. Furthermore, we show that the minimal path serves also to minimize the total entropy production occurring during the transfer of states. Finally, upon evaluating the entropic speed as well as the total entropy production along optimal transfer paths within several scenarios of physical interest in analog quantum searching algorithms, we demonstrate in a transparent quantitative manner a correspondence between a faster transfer and a higher rate of entropy production. We therefore conclude that higher entropic speed is associated with lower entropic efficiency within the context of quantum state transfer.

PACS numbers: Information Theory (89.70.+c), Probability Theory (02.50.Cw), Quantum Computation (03.67.Lx), Quantum Information (03.67.Ac), Quantum Mechanics (03.65.-w), Riemannian Geometry (02.40.Ky), Statistical Mechanics (05.20.-y).

I. INTRODUCTION

Understanding the intersection between thermodynamics and quantum mechanics is becoming increasingly relevant, especially at the nanoscale level, since applications such as quantum computing are moving from the theoretical arena to real world applications. In particular, the necessity of designing quantum algorithms that are not simply faster, but also optimized from a thermodynamical standpoint, is becoming increasingly evident [1–4]. Because of this, it is insightful to study algorithms such as analog quantum search algorithms using geometric ideas, which are of great interest in both quantum mechanics and thermodynamics alike.

The idea of fluctuations is central to the Riemannian geometrization of both quantum mechanics and thermodynamics. In quantum mechanics, for instance, a natural distance on the set of quantum states is represented by the angle in Hilbert space. In particular, up to a constant factor, the angle is the only Riemannian metric on the set of rays which is invariant under all possible unitary time evolutions. More importantly perhaps, Wootters showed in Ref. [5] that this natural distance is equivalent to the statistical distance defined between different preparations of the same quantum system and is determined completely by the size of statistical fluctuations occurring in quantum measurements designed to distinguish one quantum state from another. In quantum mechanics, statistical fluctuations are unavoidable and are associated with a finite sample. In particular, two preparations are indistinguishable in a given number of trials if the difference in the actual probabilities is smaller than the size of a typical fluctuation. In thermodynamics, including the theory of fluctuations in the axioms of equilibrium thermodynamics [6], a natural distance on the set of equilibrium thermodynamic states is given in terms of a positive-definite Riemannian metric proportional to the second order partial derivative of the total entropy of the thermodynamic system and the reservoir with which it is in contact [7, 8]. Roughly speaking, according to the theory of fluctuations, when a thermodynamic system is in contact with a reservoir, it reaches a steady-state condition in finite time by thermally fluctuating among a continuous sequence of intermediate states. In particular, the physical interpretation of distance between two thermodynamic states can be described by stating that the less the probability of fluctuation between the states, the further apart they are. Therefore, in both quantum mechanics and thermodynamics, Riemannian geometric structures emerge because of the presence of fluctuations.

Furthermore, although arising from a different physical origin, either statistical fluctuations in quantum mechanics

or thermal fluctuations in thermodynamics are concepts that can be described quantitatively in terms of probabilities. Indeed, both the thermodynamic [9, 10] and the quantum [11] metric tensors can be described in a more general information-theoretic setting in terms of the Fisher information [12]. This quantity is central to information geometry [13], the latter being the application of Riemannian geometry to probability calculus [14]. In particular, the Fisher information matrix is a covariance matrix that is symmetric and positive semi-definite. Therefore, it can be employed as a metric tensor to define a notion of distance between points (for instance, probabilities, pure states, or density operators) in the space of parameters.

In the framework of finite-time thermodynamic processes controlled by external reservoirs [9, 15–17], Riemannian geometric methods have been used to find the best path in the state space along which one drives the thermodynamic system from a given equilibrium state to another. Specifically, using the concepts of thermodynamic length and thermodynamic divergence of a path, it was shown that the optimum cooling paths (that is, paths of minimum entropy production) correspond to geodesic motion with constant thermodynamic speed in the Riemann-metricized manifold of thermodynamic states [18, 19]. In recent years, the concept of thermodynamic length, adapted to the framework of nanoscale processes [10, 20, 21], has been used in a number of works to find optimal control parameter protocols in simple non-equilibrium models. In this context, optimum paths are geodesics on the parameter manifold and are non-equilibrium control protocols with lowest achievable dissipation [22, 23]. Moreover, inspired by Jaynes’ information-theoretic reformulation of statistical mechanics [24, 25], Frieden and collaborators discussed the role played by the Fisher information in both equilibrium and non-equilibrium thermodynamics in Refs. [26–28].

Within the context of quantum search algorithms [29, 30], Riemannian geometric concepts have been employed to facilitate novel modeling and analyses across a diverse range of differing approaches. In [31] for instance, it was demonstrated that Grover’s search algorithm can be specified via a unitary, adiabatic process that leaves the Fisher information function invariant. In [32] on the other hand, the role of entanglement in quantum searching was investigated from the perspective of the Fubini-Study metric. Further still, upon quantifying the concept of quantum distinguishability among parametric density operators by means of the Wigner-Yanase quantum information metric in [33, 34], it was demonstrated that the problem of quantum searching can be reformulated in an information geometric setting, wherein Grover’s dynamics can be characterized by geodesic curves on the parametric manifold of pure quantum state density operators. These density operators in turn, are obtained from the continuous approximation of parametric quantum output states of Grover’s search algorithm. Finally, in Ref. [35], information geometric techniques were used to confirm the superfluous nature of the Walsh-Hadamard operation and, more significantly, to reproduce the relation describing quadratic speed-up.

The thermodynamical perspectives on quantum computation and information provided by [36] and [37], respectively, together with that on quantum error correction provided by [38, 39], can prove deeply informative. When viewed in the context of simple quantum circuit models, the performance of search schemes in the framework of both classical and quantum algorithms is usually quantified in terms of the so-called query complexity of the algorithm. By query complexity we refer to the number of oracle queries implemented by the algorithm. Increasingly realistic models of computation must be considered in an effort to properly analyze quantum speed-ups. Among other aspects, physically realistic analyses should take account of the thermodynamical (resource) costs of implementing such algorithms on actual computer hardware. Several initial results appear in [40, 41]. By making use of Bennett’s Brownian model of reversible, low power computation [36] for instance, Perlner and Liu argued in Ref. [41] that exhaustive classical searching can be robustly competitive with Grover’s algorithm when the comparison between the two quantum searching protocols is made in terms of actual thermodynamical (resource) costs including memory size, energy consumption and computation time. The comparative analysis presented in Ref. [41] focuses entirely upon the comparison between Grover’s quantum search algorithm and classical search schemes. We remark that a comparison among alternative quantum search protocols is absent in Ref. [41].

An information geometric description of monotonic and oscillatory behavior of (statistically) parametrized squared probability amplitudes arising from Fisher information functional forms that are selected *ad hoc*, namely constant, power-law and exponential decay, was presented in Ref. [42]. For each of these cases, the speed as well as thermodynamic divergence of the associated physical processes was computed by utilizing a useful Riemannian geometrization of relevant thermodynamical concepts. Furthermore, we discussed in brief the possibility of leveraging our proposed information geometric framework to characterize a compromise between thermodynamic efficiency and speed in quantum searching protocols. One primary limitation of the analysis presented in Ref. [42] is the fact that the Fisher information functional forms were selected in an *ad hoc* manner without prescribing their emergence from a well defined underlying physical setting. Despite the mathematical generality however, the predicted behaviors of the parametrized squared probability amplitudes that arise from our information geometric modeling lacks any clear physical interpretation. Motivated by the results of Byrnes and collaborators [43], we presented in Ref. [44] an in-depth analysis describing the physical relationship between analytically soluble two-level time-dependent quantum systems and quantum search Hamiltonians. In particular, we calculated in an exact analytical manner the transition probabilities from a source state to target state in several physical scenarios featuring a spin-1/2 test particle immersed

in an external time-dependent magnetic field. To be more specific, we investigated both the monotonic as well as the periodic oscillatory temporal behaviors of such transition probabilities and moreover, investigated their analogy with intrinsic features of both fixed-point and Grover-like quantum searching protocols, respectively. Finally, we discussed from a physical perspective the relationship that exists between the schedule of a quantum searching algorithm in both adiabatic and non-adiabatic quantum evolutions, and the control magnetic fields present in time-dependent driving Hamiltonians.

In this paper, driven by the absence of any thermodynamical analysis of quantum searching protocols and building upon our previous research presented in Refs. [42, 44–48], we incorporate the Riemannian geometric concepts of speed and efficiency within both thermodynamical and quantum mechanical settings, in an effort to provide some theoretical perspective on the compromise between efficiency and speed in terms of minimal entropy production channels arising from quantum evolutions. In particular, we present an information geometric characterization of entropy production rates and entropic speeds in geodesic evolution occurring on statistical manifolds of parametrized quantum states, which emerge as output states of $\mathfrak{su}(2; \mathbb{C})$ Hamiltonian models that approximate various types of continuous-time quantum search protocols. Before describing how the present article is organized, we emphasize that our work being presented here is a more in depth unabridged version of Ref. [46] and is more suitable for an audience with a broader interest in mathematical methods in theoretical physics.

The layout of this article is as follows: in Section II, we present several relevant and useful information geometric concepts. Among others, we direct our attention to the notions of Fisher information, thermodynamic divergence and thermodynamic length. In Section III, we clarify in precise terms how the pure quantum states that we consider arise as outputs of suitably chosen $\mathfrak{su}(2; \mathbb{C})$ time-dependent Hamiltonian operators used to describe differing types of analog quantum searching algorithms. In Section IV, we introduce the positive definite (i.e. Riemannian) metrization of the parameter manifold, where the latter is specified by the Fisher information functional evaluated along parametrized squared probability amplitudes. Our concluding remarks are presented in Section V.

II. PRELIMINARIES IN INFORMATION GEOMETRY

In this section we introduce some preliminaries in the study of information geometry, particularly the concepts of Fisher information, thermodynamic length, and thermodynamic divergence.

A. Fisher information

1. Fisher information in information theory

Assume X to be a discrete random variable with alphabet \mathcal{X} , and let $p_X(x; \theta) = p_x(\theta)$ be the probability mass function for X that depends on a single parameter θ . The Fisher information $\mathcal{F}(\theta)$ quantifies how much information X contains about the parameter θ . In other words, it provides a lower bound on the error in estimating the value of θ from the data in X . Formally, in the single-parameter case, it is defined as the variance of the score $V \stackrel{\text{def}}{=} \partial_\theta \{\log[p_x(\theta)]\}$, namely

$$\mathcal{F}(\theta) \stackrel{\text{def}}{=} \text{var}(V) = E_\theta \left[\{\partial_\theta \log[p_x(\theta)]\}^2 \right], \quad (1)$$

where $E_\theta[\cdot]$ denotes the expected value with respect to $p_x(\theta)$ and $\partial_\theta \stackrel{\text{def}}{=} \partial/\partial\theta$. As a side remark, we point out that the mean value of the score is zero. Then, given any unbiased estimator $T(X)$ of the parameter θ , the Cramer-Rao inequality states that the mean-squared error of $T(\theta)$ is lower bounded by the reciprocal of the Fisher information [12],

$$\text{var}(T) \geq \frac{1}{\mathcal{F}(\theta)}. \quad (2)$$

In the case where $p_x(\theta)$ depends on multiple parameters $\theta \stackrel{\text{def}}{=} (\theta^1, \dots, \theta^M)$, the Fisher information is a matrix with elements $\mathcal{F}_{\alpha\beta}(\theta)$, defined by

$$\mathcal{F}_{\alpha\beta}(\theta) \stackrel{\text{def}}{=} E_\theta [(V_\alpha - \langle V_\alpha \rangle) (V_\beta - \langle V_\beta \rangle)], \quad (3)$$

where $\langle V_\alpha \rangle \stackrel{\text{def}}{=} E_\theta [V_\alpha]$ and $V_\alpha \stackrel{\text{def}}{=} \partial_\alpha \{\log [p_x(\theta)]\}$ with $\partial_\alpha \stackrel{\text{def}}{=} \partial/\partial\theta^\alpha$. Alternatively, Eq. (3) can be recast as,

$$\mathcal{F}_{\alpha\beta}(\theta) \stackrel{\text{def}}{=} \sum_{x \in \mathcal{X}} p_x(\theta) \frac{\partial \log [p_x(\theta)]}{\partial \theta^\alpha} \frac{\partial \log [p_x(\theta)]}{\partial \theta^\beta}. \quad (4)$$

with “log” denoting the natural logarithm. Finally, we can extend this definition to the case of a continuous random variable X with alphabet \mathcal{X} and probability density function $\rho_X(x; \theta)$. Then the quantity $\mathcal{F}_{\alpha\beta}(\theta)$ in Eq. (4) becomes [12]

$$\mathcal{F}_{\alpha\beta}(\theta) \stackrel{\text{def}}{=} \int_{\mathcal{X}} \rho_X(x; \theta) \frac{\partial \log [\rho_X(x; \theta)]}{\partial \theta^\alpha} \frac{\partial \log [\rho_X(x; \theta)]}{\partial \theta^\beta} dx. \quad (5)$$

The Fisher information is a central idea in not only the fields of information theory [12] and information geometry [13], but also in the geometric descriptions of both quantum mechanics [11, 49] and statistical mechanics [50].

2. Fisher information in quantum mechanics

From a quantum mechanical viewpoint, consider an $N \stackrel{\text{def}}{=} 2^n$ -dimensional complex Hilbert space \mathcal{H}_2^n . Furthermore, consider two neighboring normalized pure states $|\psi(\theta)\rangle$ and $|\psi'(\theta)\rangle$ expanded with respect to an orthonormal basis $\{|k\rangle\}$ with $1 \leq k \leq N$,

$$|\psi\rangle \stackrel{\text{def}}{=} \sum_{k=1}^N \sqrt{p_k} e^{i\varphi_k} |k\rangle \quad \text{and} \quad |\psi'\rangle \stackrel{\text{def}}{=} \sum_{k=1}^N \sqrt{p_k + dp_k} e^{i(\varphi_k + d\varphi_k)} |k\rangle, \quad (6)$$

where $p_k = p_k(\theta)$ and $\varphi_k = \varphi_k(\theta)$ with θ being a continuous real parameter. The quantum distinguishability metric on this manifold of Hilbert space rays is given by the Fubini-Study metric [11],

$$ds_{\text{FS}}^2 \stackrel{\text{def}}{=} \left\{ \cos^{-1} [|\langle \psi' | \psi \rangle|] \right\}^2 = g_{\alpha\beta}^{(\text{FS})}(\theta) d\theta^\alpha d\theta^\beta, \quad (7)$$

where the Fubini-Study metric tensor components $g_{\alpha\beta}^{(\text{FS})}$ are related to the Fisher-Rao metric tensor components $\mathcal{F}_{\alpha\beta}(\theta)$ by the relation

$$g_{\alpha\beta}^{(\text{FS})}(\theta) = \frac{1}{4} [\mathcal{F}_{\alpha\beta}(\theta) + 4\sigma_{\alpha\beta}^2(\theta)]. \quad (8)$$

The quantities $\mathcal{F}_{\alpha\beta}(\theta)$ and $\sigma_{\alpha\beta}^2(\theta)$ in Eq. (8) are formally defined as,

$$\mathcal{F}_{\alpha\beta}(\theta) \stackrel{\text{def}}{=} \sum_{k=1}^N \frac{1}{p_k(\theta)} \frac{\partial p_k(\theta)}{\partial \theta^\alpha} \frac{\partial p_k(\theta)}{\partial \theta^\beta}, \quad (9)$$

and,

$$\sigma_{\alpha\beta}^2(\theta) \stackrel{\text{def}}{=} \sum_{k=1}^N \frac{\partial \varphi_k(\theta)}{\partial \theta^\alpha} \frac{\partial \varphi_k(\theta)}{\partial \theta^\beta} p_k(\theta) - \left(\sum_{k=1}^N \frac{\partial \varphi_k(\theta)}{\partial \theta^\alpha} p_k(\theta) \right) \left(\sum_{k=1}^N \frac{\partial \varphi_k(\theta)}{\partial \theta^\beta} p_k(\theta) \right), \quad (10)$$

respectively. In what follows, we shall assume that the non-negative term $\sigma_{\alpha\beta}^2(\theta)$ in Eq. (10) related to the variance of the phase changes is equal to zero. This assumption is valid by rephasing in a convenient manner the basis vectors used to express the state $|\psi(\theta)\rangle$ (for details, we refer to Ref. [11] and Ref. [42]). In particular, the rephasing procedure requires that $\text{Im}[\langle \psi(\theta) | k \rangle \langle k | d\psi_\perp(\theta) \rangle] = 0$, for any $1 \leq k \leq N$. The state $|d\psi_\perp\rangle \stackrel{\text{def}}{=} |d\psi\rangle - \langle \psi | d\psi \rangle |d\psi\rangle$ is the projection of $|d\psi\rangle$ orthogonal to $|\psi\rangle$ where $|d\psi\rangle \stackrel{\text{def}}{=} |\psi'\rangle - |\psi\rangle$ while $|\psi\rangle$ and $|\psi'\rangle$ are defined in Eq. (6). In summary, for a convenient choice of the basis vectors $\{|k\rangle\}$ used for the decomposition in Eq. (6), $g_{\alpha\beta}^{(\text{FS})}(\theta)$ becomes proportional to $\mathcal{F}_{\alpha\beta}(\theta)$ as evident from Eq. (8). As mentioned earlier, we refer to Ref. [11] for further details.

Interestingly, after some manipulations, the classical Fisher information in Eq. (5) can be recast in terms of probability amplitudes $\sqrt{\rho_X(x; \theta)}$,

$$\mathcal{F}_{\alpha\beta}^{(\text{classical})}(\theta) = 4 \int \partial_\alpha \sqrt{\rho_X(x; \theta)} \partial_\beta \sqrt{\rho_X(x; \theta)} dx, \quad (11)$$

where $\partial_\alpha \stackrel{\text{def}}{=} \partial/\partial\theta^\alpha$. Although quantum extensions of the Fisher information are not unique, a simple generalization of Eq. (11) occurs upon replacing the probability density function $\rho_X(x; \theta)$ by the density operator $\rho_\theta(x)$ and the integral by the trace [51, 52],

$$\mathcal{F}_{\alpha\beta}^{(\text{QM})}(\theta) = 4\text{tr} \left[\partial_\alpha \sqrt{\rho_\theta(x)} \partial_\beta \sqrt{\rho_\theta(x)} \right]. \quad (12)$$

The metric tensor in Eq. (12) is known as the Wigner-Yanase metric and is simply four times the Fubini-Study metric tensor. For a quantum mechanical evolution specified by the unitary evolution operator $\mathcal{U} \stackrel{\text{def}}{=} e^{-\frac{i}{\hbar}\mathcal{H}t}$ with $\mathcal{H}(t) \stackrel{\text{def}}{=} -i\hbar(\partial_t \mathcal{U}^\dagger)\mathcal{U}$, the quantum Fisher information is proportional to the dispersion of the Hermitian operator \mathcal{H} [53, 54],

$$\mathcal{F}^{(\text{QM})}(t) = \frac{4}{\hbar^2} \langle \Delta \mathcal{H}^2(t) \rangle. \quad (13)$$

In Eq. (13), $\Delta \mathcal{H} \stackrel{\text{def}}{=} \mathcal{H} - \langle \mathcal{H} \rangle$ with $\langle \mathcal{H} \rangle$ denoting the expectation value of the operator \mathcal{H} with respect to the initial state of the quantum system. While the Fubini-Study metric is defined on the space of pure states, the non-uniqueness of the quantum Fisher metric becomes especially meaningful when considering quantum mixed states [55]. In the framework of mixed density operators, it is particularly convenient to introduce the Bures line element ds_{Bures}^2 [56],

$$ds_{\text{Bures}}^2 \stackrel{\text{def}}{=} 2[1 - F(\rho, \rho + d\rho)]. \quad (14)$$

In Eq. (14), the quantity $F(\rho, \sigma) \stackrel{\text{def}}{=} \text{tr} \sqrt{\rho^{1/2} \sigma \rho^{1/2}}$ denotes the so-called Uhlmann fidelity [57]. In particular, we point out that ds_{Bures}^2 reduces to ds_{FS}^2 for pure states.

Interestingly, the Ising model is an ideal testing ground for the convergence of both statistical inference and information geometric methods applied to thermodynamical reasoning [58]. Indeed, within the quantum setting, a very interesting link between quantum information geometry and thermodynamics arises in the study of the Bures metric on thermal state manifolds corresponding to the quantum Ising model [59],

$$ds_{\text{Bures}}^2 \stackrel{\text{def}}{=} \frac{1}{4} \langle \Delta \mathcal{H}^2(t) \rangle d\beta^2 = \frac{1}{4} T^2 C_v d\beta^2. \quad (15)$$

In Eq. (15), T is the temperature, C_v is the specific heat, and $\langle \cdot \rangle$ denotes the expectation value with respect to thermal Gibbs states. For further details, we refer to Ref. [59].

3. Fisher information in statistical mechanics

After some straightforward manipulations of Eq. (5), it can be shown that the Fisher metric tensor in Eq. (5) can be recast as [60],

$$\mathcal{F}_{\alpha\beta}(\theta) \stackrel{\text{def}}{=} - \left(\frac{\partial^2 \mathcal{S}(\theta, \theta')}{\partial \theta'^\alpha \partial \theta'^\beta} \right)_{\theta'=\theta} = -E_\theta [\partial_{\alpha\beta}^2 \log \rho_X(x; \theta)], \quad (16)$$

where $\mathcal{S}(\theta, \theta')$ is the so-called logarithmic relative entropy,

$$\mathcal{S}(\theta, \theta') \stackrel{\text{def}}{=} - \int_{\mathcal{X}} \rho_X(x; \theta) \log \left[\frac{\rho_X(x; \theta)}{\rho_X(x; \theta')} \right] dx. \quad (17)$$

For the sake of completeness, we remark that by defining the logarithmic relative entropy by means of the natural logarithmic function, its numerical value is expressed in units of “nats” where $1 \text{ nat} \stackrel{\text{def}}{=} [\log(2)]^{-1}$ bits. Therefore, the temporal entropy rate would be measured in nats/sec. Furthermore, from a statistical mechanical standpoint, the thermodynamic metric tensor $g_{\alpha\beta}^{(\text{thermo})}(\theta)$ is defined as [10],

$$g_{\alpha\beta}^{(\text{thermo})}(\theta) \stackrel{\text{def}}{=} \frac{\partial^2 \psi}{\partial \theta^\alpha \partial \theta^\beta} = E_\theta [(X_\alpha - \langle X_\alpha \rangle)(X_\beta - \langle X_\beta \rangle)], \quad (18)$$

where $\psi \stackrel{\text{def}}{=} \log(\mathcal{Z})$ is the Massieu thermodynamic potential (that is, the free entropy) with \mathcal{Z} being the partition function of the particular statistical mechanical system being considered. To understand the identity between $\mathcal{F}_{\alpha\beta}(\theta)$

Theoretical Arena	Parameter of Interest	Fluctuating Observable	Fisher Information	Length
information theory	elapsed time	score function	variance of the score	entropic
thermodynamics	temperature	energy	size of energy fluctuations	thermodynamic
quantum theory	magnetic field intensity	Hermitian operator	dispersion of the operator	statistical

TABLE I: Illustrative representation of common parameters of interest and fluctuating observables together with the physical interpretation of Fisher information and length through parameter space in information theory, thermodynamics, and quantum theory.

in Eq. (16) and $g_{\alpha\beta}^{(\text{thermo})}(\theta)$ in Eq. (18), consider a probability distribution given by the Gibbs equilibrium ensemble

$$\rho_X(x; \theta) \stackrel{\text{def}}{=} \exp \left[c(x) + \sum_{i=1}^M \theta^i X_i(x) - \psi(\theta) \right], \quad (19)$$

with $c(x)$ and $X_i(x)$ being smooth functions on \mathcal{X} . Substituting Eq. (19) into Eq. (18), we obtain

$$g_{\alpha\beta}^{(\text{thermo})}(\theta) = -E_\theta [\partial_{\alpha\beta}^2 \log \rho_X(x; \theta)]. \quad (20)$$

Therefore, from Eqs. (20) and (16), we conclude that the thermodynamic metric tensor is identical to the Fisher metric tensor [10]. Indeed, the justification of this identity is rooted in the fact that the statistical definition of entropy is more general than the original thermodynamic definition. For an overview of the physical meaning of the Fisher information in information theory, quantum mechanics, and thermodynamics, we refer to Table I.

B. Thermodynamic length and divergence

We have seen that given a space of states, we can employ a suitable Riemannian metric tensor to define the distance between states and thus the length of paths between states. Points in this state space may represent statistical distributions (as in Eq. (5)), quantum state vectors (as in Eq. (8)), or thermodynamic states (as in Eq. (18)). A generalized concept that provides a convenient parametrization for these types of spaces is the information-theoretic notion of entropy, which allows one to use the Fisher metric tensor as a metric on the state space, such as in Eq. (16). We have seen that this perspective not only allows one to consider parameters more general than those typically used in thermodynamics, but also makes transparent the connections between state spaces in these different fields.

Riemannian metrics on thermodynamic equilibrium state spaces can be achieved in a number of ways. Weinhold's approach [61] used the second derivatives of internal energy with respect to extensive variables, while Ruppeiner's approach [7] used the second derivatives of the entropy as a function of extensive variables. These extensive variables could be, for example, volume or mole number. These approaches were shown to be conformally equivalent by Salamon and collaborators in Ref. [62]. Using the energy approach, Salamon and Berry defined in Ref. [15] the length of a path γ_θ in the space of thermal states as follows,

$$\mathcal{L}(\tau) \stackrel{\text{def}}{=} \int_0^\tau \sqrt{\frac{d\theta^\alpha}{d\xi} g_{\alpha\beta}(\theta) \frac{d\theta^\beta}{d\xi}} d\xi, \quad (21)$$

where the parameter θ depends on an affine parameter ξ with $0 \leq \xi \leq \tau$, and $g_{\alpha\beta}(\theta)$ is the thermodynamic metric tensor introduced in Eq. (18). The quantity $\mathcal{L}(\tau)$, with physical dimensions of $(\text{energy})^{1/2}$, is called the “thermodynamic length” of the path γ_θ . Similarly, one can define this length using the entropy approach, in which case the “entropy” lengths would differ from the “energy” lengths by a factor of the square root of some average temperature throughout the thermodynamic process under consideration [15, 62]. The length computed using the thermodynamic entropy approach in the space of extensive variables can also be shown, under suitable working conditions, to be equal to the length computed using the entropy of a probability distribution in the space of parameters for the distribution [9]. Along with the thermodynamic length of a path, it is also useful to introduce the so-called thermodynamic divergence $\mathcal{I}(\tau)$ of γ_θ , defined as [10],

$$\mathcal{I}(\tau) \stackrel{\text{def}}{=} \tau \int_0^\tau \frac{d\theta^\alpha}{d\xi} g_{\alpha\beta}(\theta) \frac{d\theta^\beta}{d\xi} d\xi. \quad (22)$$

To better understand the meaning of Eqs. (21) and (22), we note that by the Cauchy-Schwarz inequality applied to two smooth functions $f_1(t)$ and $f_2(t)$,

$$\left[\int_0^\tau f_1(t) f_2(t) dt \right]^2 \leq \left\{ \int_0^\tau [f_1(t)]^2 dt \right\} \left\{ \int_0^\tau [f_2(t)]^2 dt \right\}, \quad (23)$$

it follows that $\mathcal{I} \geq \mathcal{L}^2$. That is, the thermodynamic divergence is always greater than the square of the thermodynamic length. The special case $\mathcal{I} = \mathcal{L}^2$ occurs when the integrand in Eq. (22) is constant along the path γ_θ . The divergence \mathcal{I} is a measure of the amount of natural fluctuations along a path, while the length \mathcal{L} is a measure of the cumulative root-mean-square deviations along the path [10]. Given these facts, and given the connection between metric tensors and statistical fluctuations such as in Eqs. (3) and (18), we may view these quantities as control measures of dissipation in finite-time thermodynamic processes, making them very useful in the Riemannian geometric formulation of thermodynamics.

The Riemannian geometric formulation of thermodynamics concerns the problem of reversibly transferring a thermodynamic system from some initial state to some final state under the constraint of minimum total entropy production (or minimum loss of availability). In particular, one considers a relaxation process in which the system is driven by a sequence of $\tilde{n} \stackrel{\text{def}}{=} \tau/(\delta t)$ steps. Interestingly, when considering this problem in terms of the thermodynamic divergence along a path γ_θ defined in Eq. (22), it can be shown that this quantity equals the total entropy production (dissipation) of the path in the continuum limit of a sequence of step equilibrations [9, 10, 18]. That is, in the limit that δt approaches zero (and the number of steps \tilde{n} approaches infinity), the process is ideally reversible. This has found use in the study of control parameter protocols that minimize dissipation in molecular machines, in which the Riemannian manifold is induced by a friction tensor and the thermodynamic divergence is proportional to the average excess work performed during the protocol [20, 23].

C. Optimum paths: Speed and Efficiency

The problem is therefore to find the optimum paths γ_θ that minimize an action functional given by the length \mathcal{L} in Eq. (21). Let $\theta \stackrel{\text{def}}{=} \{\theta^\alpha\}$, $1 \leq \alpha \leq M$ constitute the parameter space, where M is the dimensionality of the space, and let γ_θ be defined by $\theta(\xi)$ with $0 \leq \xi \leq \tau$. Then the minimum length path occurs under some optimal affine time parametrization ξ (unique up to a change of scale and origin). Quantitatively, by using variational calculus and tensor algebra, requiring that $\delta\mathcal{L} = 0$ and imposing the requirement that $\delta\theta^\alpha = 0$ at the extrema of the path leads to the familiar geodesic equations,

$$\frac{d^2\theta^\alpha}{d\xi^2} + \Gamma_{\beta\gamma}^\alpha \frac{d\theta^\beta}{d\xi} \frac{d\theta^\gamma}{d\xi} = 0, \quad (24)$$

where the quantities $\Gamma_{\beta\gamma}^\alpha$ are the Christoffel connection coefficients of the second kind, defined as [63],

$$\Gamma_{\beta\gamma}^\alpha \stackrel{\text{def}}{=} \frac{1}{2} g^{\alpha\delta} (\partial_\beta g_{\delta\gamma} + \partial_\gamma g_{\beta\delta} - \partial_\delta g_{\beta\gamma}), \quad (25)$$

with $\partial_\beta \stackrel{\text{def}}{=} \partial/\partial\theta^\beta$. By considering the Fisher information matrix elements $\mathcal{F}_{\alpha\beta}(\theta)$ in Eq. (3) as the components of the metric tensor $g_{\alpha\beta}(\theta)$, the geodesic equations in Eq. (24) become,

$$\frac{d^2\theta^\alpha}{d\xi^2} + \frac{1}{2} \mathcal{F}^{\alpha\beta}(\theta) [\partial_\nu \mathcal{F}_{\beta\rho}(\theta) + \partial_\rho \mathcal{F}_{\nu\beta}(\theta) - \partial_\beta \mathcal{F}_{\nu\rho}(\theta)] \frac{d\theta^\nu}{d\xi} \frac{d\theta^\rho}{d\xi} = 0. \quad (26)$$

Interestingly, if we decide instead to minimize the thermodynamic divergence $\mathcal{I}(\tau)$ under the same working assumptions, the geodesic equations become,

$$\frac{d}{d\xi} \left[\mathcal{F}_{\alpha\rho}(\theta) \frac{d\theta^\alpha}{d\xi} \right] - \frac{1}{2} \frac{d\theta^\alpha}{d\xi} \frac{\partial \mathcal{F}_{\alpha\beta}(\theta)}{\partial \theta^\rho} \frac{d\theta^\beta}{d\xi} = 0, \quad (27)$$

which can readily be shown to yield identical geodesic paths to the equations in Eq. (26). That is to say, optimal paths minimizing the thermodynamic length are also paths that minimize the thermodynamic divergence. We also remark that Eq. (27) is the information geometric analogue of Eq. (36) in Ref. [18] and Eq. (6) in Ref. [23]. By

exploiting the concept of geodesic paths, we can define the “thermodynamic” speed (henceforth referred to as entropic speed v_E) as

$$v_E \stackrel{\text{def}}{=} \sqrt{\frac{d\theta^\alpha}{d\xi} g_{\alpha\beta}(\theta) \frac{d\theta^\beta}{d\xi}}, \quad (28)$$

which is constant along these optimum paths. Optimum paths also have a constant rate of entropy production r_E , given by

$$r_E \stackrel{\text{def}}{=} \frac{d\mathcal{I}}{d\tau}, \quad (29)$$

where $\mathcal{I}(\tau)$ is evaluated along an optimal path. This quantity is identical to the squared invariant norm of the speed v_E when considering an optimal path. We use the term “entropic” speed since the statistical definition of entropy is more general than the original thermodynamic definition, as previously discussed. We will therefore refer to lengths and divergences as “entropic” quantities as well in future discussions.

We emphasize that v_E in Eq. (28) has analogues in both thermodynamics and quantum mechanics. In thermodynamics, the thermodynamic speed v_{thermo} is defined as the natural-time derivative of the thermodynamic length \mathcal{L} computed from the entropy version of the metric tensor, and is given by [64],

$$v_{\text{thermo}} \stackrel{\text{def}}{=} \frac{d\mathcal{L}}{d\xi}, \quad (30)$$

where the dimensionless natural time scale ξ (sometimes referred to as thermodynamic time) is defined in terms of the clock time t , the temperature T of the system, and the relaxation time $\epsilon(T)$ as follows,

$$d\xi \stackrel{\text{def}}{=} \frac{dt}{\epsilon(T)}. \quad (31)$$

In quantum mechanics on the other hand, the statistical speed v_{stat} is defined as the rate of change of the absolute statistical distance $l(\theta)$ between two states (either pure states in Hilbert space or mixed states in the space of density operators) along the path parametrized by θ , given by [5, 11],

$$v_{\text{stat}} \stackrel{\text{def}}{=} \frac{dl(\theta)}{d\theta}, \quad (32)$$

where $dl^2(\theta) \stackrel{\text{def}}{=} g_{\alpha\beta}^{(\text{FS})}(\theta) d\theta^\alpha d\theta^\beta$ with $g_{\alpha\beta}^{(\text{FS})}(\theta)$ given by Eq. (8). The absolute statistical distance $l(\theta)$ is interpreted as the maximum number of distinguishable quantum states along the path parametrized by θ optimized over all possible generalized quantum measurements (that is, under the most discriminating measurements). The Eq. (32) also provides an intuitive physical interpretation for the quantum Fisher information as the square root of the statistical speed [54, 65, 66].

In the final paragraph of this section, we propose an information geometric notion of entropic efficiency. We recall that the thermal efficiency η_{thermo} of a heat engine in thermodynamics is defined as [67],

$$\eta_{\text{thermo}} \stackrel{\text{def}}{=} 1 - \frac{Q_{\text{out}}}{Q_{\text{in}}}. \quad (33)$$

In Eq. (33), Q_{out} and Q_{in} denote the output and input thermal energies with $W_{\text{out}} \stackrel{\text{def}}{=} Q_{\text{in}} - Q_{\text{out}}$ being the actual work performed by the heat engine. We also point out that heat resistance, friction, internal losses, and heat leakage are some factors that can cause deviations from ideality in real heat engines. For a minimum entropy production analysis in a heat engine subject to thermal-resistance losses, we refer to Ref. [68]. Furthermore, for recent important works on the existence of a universal trade-off between efficiency and power in heat engines, we refer to Refs. [69, 70]. Finally, the efficiency of a quantum evolution in the Riemannian approach to quantum mechanics is defined as [71],

$$\eta_{\text{QM}} \stackrel{\text{def}}{=} 1 - \frac{\Delta s}{s}, \quad (34)$$

with $0 \leq \eta_{\text{QM}} \leq 1$ and $\Delta s \stackrel{\text{def}}{=} s - s_0$. The quantity s_0 denotes the dimensionless distance along the shortest geodesic γ_{shortest} joining the fixed initial ($|\psi_i\rangle$) and final ($|\psi_f\rangle$) points of the evolution that are distinct points on the complex projective Hilbert space. The quantity s instead, is the distance along a given path γ connecting $|\psi_i\rangle$ and $|\psi_f\rangle$ and

is measured by the Fubini-Study metric. We remark that s does not depend on the specific Hamiltonian used to transport the quantum state along the given path. It depends only on the unparametrized curve γ in the projective Hilbert space that is determined by the quantum evolution. The quantum evolution is maximally efficient when the evolution occurs with minimum time-energy uncertainty. This scenario is characterized by $\eta_{\text{QM}} = 1$ and is actualized when γ and s approach γ_{shortest} and s_0 , respectively.

In analogy to these definitions of efficiency in thermodynamics and quantum mechanics, we find it useful to define entropic efficiency based on the notion of minimum entropy production as opposed to minimum energy dispersion. Given an initial and final point on an information manifold, there is a set of distinct evolutions with entropy production rates $r_E^{(i)} \in \mathbb{R}_+ \setminus \{0\}$, where the index “ i ” labels each evolution. We define the entropic efficiency of a particular evolution between those two points as,

$$\eta_E \stackrel{\text{def}}{=} 1 - \frac{r_E}{r}, \quad (35)$$

where $r \stackrel{\text{def}}{=} \left\lceil \left[r_E^{(i)} \right] \right\rceil$ is the maximum of the ceiling functions of the entropy production rates of the different paths. By ceiling function, we mean the function mapping $x \in \mathbb{R}$ to the least integer greater than or equal to x . The quantity r is a normalizing factor that can be interpreted as the least integer upper bound of the entropy production rate of the hottest among all cool paths available for the evolution between two points. It ensures that the quantity η_E has the key properties of being adimensional and satisfying $0 \leq \eta \leq 1$. The ideal value $\eta = 1$ is achieved when the evolution corresponds to a path whose entropy production remains ideally constant, and is therefore maximally cooled or maximally reversible. We remark that in such a case, just as the quantum mechanical efficiency η_{QM} approaches 1 as $\Delta s \rightarrow 0$, so too does the quantity η_E approach 1 as $r_E \rightarrow 0$.

Building on the preliminary concepts introduced in this section, we will describe in the next section the particular quantum mechanical evolutions that generate the probability paths to which we will apply these notions of speed and minimum entropy production from an information geometric viewpoint.

III. $\text{SU}(2; \mathbb{C})$ HAMILTONIAN MODELS

In this section, we show how the pure states we consider can result from evolution under a suitably defined $\text{su}(2; \mathbb{C})$ time-dependent Hamiltonian operator. These pure states are useful for understanding various types of analog quantum search strategies using physical reasoning [44, 45].

A. Hamiltonian evolution

We start with a time-dependent Hamiltonian operator $\mathcal{H}_{\text{su}(2; \mathbb{C})}(t)$ defined in terms of three anti-Hermitian and traceless generators of $\text{su}(2; \mathbb{C})$, the Lie algebra of the special unitary group $\text{SU}(2; \mathbb{C})$ [72]. These generators are $\{i\sigma_x, -i\sigma_y, i\sigma_z\}$, where $\vec{\sigma} \stackrel{\text{def}}{=} (\sigma_x, \sigma_y, \sigma_z)$ is the familiar Pauli vector operator [73, 74]. We write $\mathcal{H}_{\text{su}(2; \mathbb{C})}(t)$ as a linear superposition of these generators in terms of complex, time-dependent coefficients ($a(t), b(t), c(t) \in \mathbb{C}$),

$$\mathcal{H}_{\text{su}(2; \mathbb{C})}(t) \stackrel{\text{def}}{=} a(t) (i\sigma_x) + b(t) (-i\sigma_y) + c(t) (i\sigma_z). \quad (36)$$

If we set $a(t) \stackrel{\text{def}}{=} -i\omega_x(t)$, $b(t) \stackrel{\text{def}}{=} i\omega_y(t)$, and $c(t) \stackrel{\text{def}}{=} -i\Omega(t)$, we have,

$$\mathcal{H}_{\text{su}(2; \mathbb{C})}(t) \stackrel{\text{def}}{=} \omega_x(t) \sigma_x + \omega_y(t) \sigma_y + \Omega(t) \sigma_z. \quad (37)$$

Defining $\omega(t) \stackrel{\text{def}}{=} \omega_x(t) - i\omega_y(t) = \omega_{\mathcal{H}}(t) e^{i\phi_{\omega}(t)}$, we have recast the Hamiltonian in terms of the so-called transverse field $\omega(t)$ and longitudinal field $\Omega(t)$. The transverse field is a complex quantity oriented in the xy -plane, while the longitudinal field is a real quantity oriented along the z -axis. These definitions cause $\mathcal{H}_{\text{su}(2; \mathbb{C})}(t)$ to bear resemblance to the Hamiltonian of a spin-1/2 particle in a time-dependent external magnetic field. For instance, considering an electron with magnetic moment $\vec{\mu} \stackrel{\text{def}}{=} \mu_{\text{Bohr}} \vec{\sigma}$ in an external magnetic field $\vec{B}(t)$, we can recast Eq. (37) as

$$\mathcal{H}_{\text{su}(2; \mathbb{C})}(t) \stackrel{\text{def}}{=} -\vec{\mu} \cdot \vec{B}(t). \quad (38)$$

We denote by $\mu_{\text{Bohr}} \stackrel{\text{def}}{=} e\hbar/(2mc)$ the Bohr magneton which is defined in terms of the electron mass m , the elementary charge e , the speed of light c , and the reduced Planck constant \hbar . We can then find the fields $\omega(t)$ and $\Omega(t)$ in terms

of the components of the external magnetic field $\vec{B}(t)$ using the following decomposition,

$$\vec{B}(t) \stackrel{\text{def}}{=} \vec{B}_\perp(t) + \vec{B}_\parallel(t), \quad (39)$$

where $\vec{B}_\perp(t) \stackrel{\text{def}}{=} B_x(t)\hat{x} + B_y(t)\hat{y}$ and $\vec{B}_\parallel(t) \stackrel{\text{def}}{=} B_z(t)\hat{z}$. It is then clear that

$$B_x(t) = -\frac{2mc}{e\hbar}\omega_x(t), \quad B_y(t) = -\frac{2mc}{e\hbar}\omega_y(t), \quad \text{and} \quad B_z(t) = -\frac{2mc}{e\hbar}\Omega(t), \quad (40)$$

or, in terms of the field magnitudes $\omega_{\mathcal{H}}(t)$ and $\Omega_{\mathcal{H}}(t)$,

$$B_\perp(t) = \frac{2mc}{|e|\hbar}\omega_{\mathcal{H}}(t), \quad \text{and} \quad B_\parallel(t) = \frac{2mc}{|e|\hbar}\Omega_{\mathcal{H}}(t). \quad (41)$$

B. Transition Probabilities

We now turn to the highly nontrivial task of obtaining exact analytical expressions for the transition probability from an initial source state $|s\rangle$ to a final target state $|w\rangle$ under quantum mechanical evolution specified by the Hamiltonian in Eq. (38). Consider the unitary evolution operator $\mathcal{U}(t)$, satisfying $i\hbar\dot{\mathcal{U}}(t) = \mathcal{H}_{\text{su}(2; \mathbb{C})}(t)\mathcal{U}(t)$ with $\dot{\mathcal{U}} \stackrel{\text{def}}{=} \partial_t \mathcal{U}$. For convenience, we choose a basis $\{|w\rangle, |w_\perp\rangle\}$ such that $\sigma_z|w\rangle = +|w\rangle$ and $\sigma_z|w_\perp\rangle = -|w_\perp\rangle$, and write the matrix representations of $\mathcal{H}_{\text{su}(2; \mathbb{C})}(t)$ and $\mathcal{U}(t)$ in this basis as follows,

$$[\mathcal{H}_{\text{su}(2; \mathbb{C})}] \stackrel{\text{def}}{=} \begin{pmatrix} \Omega(t) & \omega(t) \\ \omega^*(t) & -\Omega(t) \end{pmatrix}, \quad \text{and} \quad [\mathcal{U}(t)] \stackrel{\text{def}}{=} \begin{pmatrix} \alpha(t) & \beta(t) \\ -\beta^*(t) & \alpha^*(t) \end{pmatrix}. \quad (42)$$

Note that $\mathcal{U}(t)$ is expressed in terms of two probability amplitudes $\alpha(t)$ and $\beta(t)$, which by the unitarity of $\mathcal{U}(t)$ must satisfy the normalization condition $|\alpha(t)|^2 + |\beta(t)|^2 = 1$. Under this evolution, a given source state $|s\rangle$, which can be written as

$$|s\rangle \stackrel{\text{def}}{=} x|w\rangle + \sqrt{1-x^2}|w_\perp\rangle, \quad (43)$$

will be mapped as follows,

$$\begin{pmatrix} x \\ \sqrt{1-x^2} \end{pmatrix} \rightarrow \begin{pmatrix} \alpha(t)x + \beta(t)\sqrt{1-x^2} \\ -\beta^*(t)x + \alpha^*(t)\sqrt{1-x^2} \end{pmatrix}, \quad (44)$$

where $x \stackrel{\text{def}}{=} \langle w|s\rangle$ denotes the quantum overlap, which can be defined to be real. The transition probability from $|s\rangle$ to $|w\rangle$ can then be straightforwardly computed as,

$$\mathcal{P}_{|s\rangle \rightarrow |w\rangle}(t) \stackrel{\text{def}}{=} |\langle w|\mathcal{U}(t)|s\rangle|^2 = |\alpha(t)|^2 x^2 + |\beta(t)|^2 (1-x^2) + [\alpha(t)\beta^*(t) + \alpha^*(t)\beta(t)]x\sqrt{1-x^2}. \quad (45)$$

Therefore, one needs to compute the probability amplitudes $\alpha(t)$ and $\beta(t)$ from the evolution operator $\mathcal{U}(t)$ in order to find an exact analytical expression for the transition probability in Eq. (45). This is in general however, a rather difficult task. In terms of the fields $\omega(t)$ and $\Omega(t)$ defined previously and using the relation $i\hbar\dot{\mathcal{U}}(t) = \mathcal{H}_{\text{su}(2; \mathbb{C})}(t)\mathcal{U}(t)$, one must solve the following coupled system of first-order ordinary differential equation with time-dependent coefficients,

$$i\hbar\dot{\alpha}(t) = \Omega(t)\alpha(t) - \omega(t)\beta^*(t), \quad \text{and} \quad i\hbar\dot{\beta}(t) = \omega(t)\alpha^*(t) + \Omega(t)\beta(t), \quad (46)$$

subject to the initial conditions $\mathcal{U}(t) = \mathcal{I}$, $\alpha(0) = 1$ and $\beta(0) = 0$. Unfortunately, this approach does not lead to exact analytical solutions in many cases.

It is well known that it is difficult to exactly solve time-dependent two-level quantum system evolutions like that described above for arbitrary magnetic field configurations. There are however, special cases that have been studied and found to have exact analytical solutions. Landau and Zener studied the case of a spin-1/2 particle immersed in a magnetic field of constant intensity and time-dependent frequency [75, 76]. In a subsequent work, Rabi considered a similar scenario involving a time-dependent magnetic field precessing around the quantized z -axis, except with constant frequency [77, 78]. Rosen and Zener have also investigated the dynamics of an electron moving in an external magnetic field with a hyperbolic secant pulse configuration, in a purely analytical manner [79]. In these scenarios,

precise expressions for the chosen magnetic fields are justified either by the physics of the system being studied or (in the case of Rosen and Zener) by the mathematical convenience leading to an analytically integrable system of coupled differential equations. For more examples of novel mathematical techniques leading to systematic approaches to solving problems of this kind, we refer to Refs. [80–82]. Despite the difficulty of analytically solving this problem in general, it is occasionally possible to obtain exact solutions given some convenient physically or mathematically motivated magnetic field configurations.

One very powerful technique often used in magnetic resonance scenarios is called the rotating coordinates technique, originally used by Rabi, Ramsey, and Schwinger. In this technique one transforms the given problem to a convenient coordinate system that rotates with the system of interest, solves the simplified problem in the new system of coordinates, then applies the inverse transformation thereby facilitating a return to the original coordinates. In this context, the new coordinates are frequently referred to as the “rotating frame”, while the original coordinates are often called the “stationary frame”. In the case of resonance experiments, the rotating frame is usually chosen to rotate about the axis defined by the magnetic field \vec{B}_\parallel with angular frequency matching that of \vec{B}_\perp . To be explicit, assume that the quantum mechanical evolution in the stationary frame is governed by the Schrödinger equation,

$$i\hbar\partial_t |\psi(t)\rangle = \mathcal{H}(t) |\psi(t)\rangle. \quad (47)$$

If we define a unitary transformation T that maps between two distinct bases $\{|\psi(t)\rangle\}$ and $\{|\psi'(t)\rangle\}$, then the evolution in the new frame of reference is governed by

$$i\hbar\partial_t |\psi'(t)\rangle = \mathcal{H}'(t) |\psi'(t)\rangle, \quad (48)$$

where $|\psi'(t)\rangle \stackrel{\text{def}}{=} T|\psi(t)\rangle$ and $\mathcal{H}'(t) \stackrel{\text{def}}{=} [T\mathcal{H}(t)T^\dagger + i\hbar(\partial_t T)T^\dagger]$. By applying this result to our generalized Hamiltonian models, we are able to consider the particular case of a transformation $T \stackrel{\text{def}}{=} e^{-i\sigma_z \frac{\phi_\omega(t)}{2}}$ that rotates coordinates by an angle $\phi_\omega(t)$ about the z -axis. Then the Hamiltonians $\mathcal{H}_{\text{su}(2; \mathbb{C})}(t)$ in Eqs. (37) and (38) become

$$\mathcal{H}'_{\text{su}(2; \mathbb{C})}(t) \stackrel{\text{def}}{=} \left[\Omega(t) + \frac{\hbar}{2} \dot{\phi}_\omega(t) \right] \sigma_z + \omega_{\mathcal{H}}(t) \sigma_x, \quad (49)$$

and,

$$\mathcal{H}'_{\text{su}(2; \mathbb{C})}(t) \stackrel{\text{def}}{=} \left[-\frac{e\hbar}{2mc} B_\parallel(t) + \frac{\hbar}{2} \dot{\phi}_\omega(t) \right] \sigma_z + \frac{e\hbar}{2mc} B_\perp(t) \sigma_x, \quad (50)$$

respectively, where $\dot{\phi}_\omega \stackrel{\text{def}}{=} d\phi_\omega/dt$. The classic Rabi scenario [72] concerns the special case where the magnetic field intensities B_\parallel and B_\perp are constant while $\phi_\omega(t) \stackrel{\text{def}}{=} \omega_0 t$ with a negative constant ω_0 . Choosing ω_0 based on the so-called static resonance condition,

$$\omega_0 = \frac{e}{mc} B_\parallel, \quad (51)$$

the Hamiltonian in Eq. (50) becomes time-independent. Therefore, the Rabi scenario provides an example whereby the rotating coordinate technique transforms a time-dependent Hamiltonian into a time-independent quantum mechanical problem. In a generalization of this scenario presented by Messina and collaborators [81, 82], the quantities B_\parallel , B_\perp , and ϕ_ω are considered to be time-dependent dynamical variables. In this case, one can impose a generalized Rabi condition,

$$\dot{\phi}_\omega(t) = -\frac{2}{\hbar} \Omega(t), \quad (52)$$

in which case the Hamiltonians in Eqs. (49) and (50) lead to a simplified but not time-independent quantum mechanical problem.

As a side remark about experimental considerations, one can understand typical values of B_\parallel and B_\perp by noting that readout in nuclear magnetic resonance (NMR) experiments usually involve measuring the time-varying magnetization of a substance under the action of an external magnetic field. Specifically, the behavior of this magnetization determines the time constants commonly denoted by T_1 and T_2 [83–85]. The quantity T_1 is the “longitudinal” (z -axis) relaxation time and represents the characteristic time for an ensemble of spin-1/2 particles to return to thermal equilibrium about the z -axis. The quantity T_2 is the “transverse” (xy -plane) relaxation time (also known as coherence time), and represents the characteristic time for spins to lose coherence about the z -axis, or for the x and y components of magnetization to average to zero. Nuclear induction experiments by Bloch and collaborators [84] used

magnetic field intensities of approximately $B_{\parallel} \simeq 1826$ G and $B_{\perp} \simeq 5$ G, with relaxation times ranging from fractions of a second to several seconds (for example, $T_1 \simeq 10^{-5}$ sec.). The large range of relaxation times can be attributed to a variety of factors, such as the electronic structure of the atoms in the substance as well as their distance, motion, and nuclear moments [84].

In our present investigation, we exploit our previous work in Ref. [44] and utilize the results of Messina and collaborators in Refs. [81, 82] to facilitate the characterization of four quantum mechanical scenarios in which transition probabilities can be obtained in an exact analytical manner. We consider the transition probability $\mathcal{P}_{|w_{\perp}\rangle \rightarrow |w\rangle}(t)$ from an initial state $|w_{\perp}\rangle$ to a final state $|w\rangle$ such that $\langle w_{\perp} | w \rangle = 0$ and without loss of generality, we assume these states to be the eigenstates of the Pauli operator σ_z (in particular, $\sigma_z |w\rangle = +|w\rangle$ and $\sigma_z |w_{\perp}\rangle = -|w_{\perp}\rangle$). In all four scenarios, we assume the physical conditions are such that

$$\dot{\phi}_{\omega}(t) = \omega_0, \text{ and } \Omega(t) = -\frac{\hbar}{2}\omega_0, \quad (53)$$

where ω_0 is a negative constant. It is worth noting that we need not have chosen this condition in particular. From a general perspective, any temporal behavior $\dot{\phi}_{\omega}(t)$ and $\Omega(t)$ that satisfies Eq. (52) would be sufficient, but we choose Eq. (53) because it appears reasonable from an experimental viewpoint. We can formally categorize the four scenarios by the time-dependent functional form of the field intensity $\omega_{\mathcal{H}}(t)$. The first case assumes a constant field intensity,

$$\omega_{\mathcal{H}}^{(1)}(t) \stackrel{\text{def}}{=} \Gamma, \quad (54)$$

which defines the original Rabi condition in which $\mathcal{P}_{|w_{\perp}\rangle \rightarrow |w\rangle}(t)$ takes the form,

$$\mathcal{P}_{|w_{\perp}\rangle \rightarrow |w\rangle}^{(1)}(t) = \sin^2\left(\frac{\Gamma}{\hbar}t\right). \quad (55)$$

In the other three cases, we consider generalized Rabi scenarios wherein the field intensity $\omega_{\mathcal{H}}(t)$ changes with time. In particular, we investigate three different time-dependent behaviors: oscillatory, power law decay, and exponential law decay. The functional form of the field intensities for these cases are given by,

$$\omega_{\mathcal{H}}^{(2)}(t) \stackrel{\text{def}}{=} \Gamma \cos(\lambda t), \omega_{\mathcal{H}}^{(3)}(t) \stackrel{\text{def}}{=} \frac{\Gamma}{(1 + \lambda t)^2} \text{ and } \omega_{\mathcal{H}}^{(4)}(t) \stackrel{\text{def}}{=} \Gamma e^{-\lambda t}, \quad (56)$$

respectively. We assume Γ to be a positive constant. Note that $\omega_{\mathcal{H}}^{(2)}(t)$ is positive when $0 \leq t \leq \pi/(2\lambda)$, whereas $\omega_{\mathcal{H}}^{(3)}(t)$ and $\omega_{\mathcal{H}}^{(4)}(t)$ are strictly positive $\forall t \in \mathbb{R}$. It can be shown that in all three of these cases, the transition probability $\mathcal{P}_{|w_{\perp}\rangle \rightarrow |w\rangle}^{(j)}(t)$ with $j \in \{2, 3, 4\}$ is given by [82],

$$\mathcal{P}_{|w_{\perp}\rangle \rightarrow |w\rangle}^{(j)}(t) = \sin^2\left[\int_0^t \frac{\omega_{\mathcal{H}}^{(j)}(t')}{\hbar} dt'\right]. \quad (57)$$

This implies that, under resonance conditions, the transition probability in all four cases only depends on the time integral of the transverse field intensity $\omega_{\mathcal{H}}(t)$.

We remark that the chosen expressions of $\omega_{\mathcal{H}}(t)$ serve to specify particular types of behavior in analog quantum search algorithms. Recall that in Grover's original search algorithm [29], the algorithm must end at a specific instant in order to succeed with high probability. An improved version of his algorithm [86] has a fixed-point property that allows the success probability to remain high even when the algorithm runs with more iterations than necessary. Both of these algorithms are digital (discrete-time) search algorithms. The first analog (continuous-time) version of Grover's quantum search algorithm was proposed by Farhi-Gutmann in Ref. [87]. Inspired by works in Refs. [43, 88], we provided a perspective on the connections between analog quantum search algorithms and the physics of two-level quantum systems in Ref. [44]. We investigated this connection in detail by means of exactly solvable time-dependent two-level quantum systems, starting from a generalized quantum search Hamiltonian originally proposed in Ref. [89]. In particular, we analytically computed the transition probabilities associated with a number of physical scenarios in which a spin-1/2 particle is immersed in an external time-dependent magnetic field. Furthermore, we analyzed the temporal behaviors of these transition probabilities (oscillatory and monotonic) in analogy with key features of different types of quantum search algorithms (Grover-like and fixed point, respectively). We then investigated the physical connection between a search algorithm's schedule and the control fields in a driving Hamiltonian in both adiabatic [90] and nonadiabatic [91] quantum mechanical evolutions. The present paper builds upon this line of investigation by specifying, in terms of the transverse field intensity $\omega_{\mathcal{H}}(t)$, the particular behavior associated with analog quantum search algorithms corresponding to the two-level system.

Rabi Scenario	Transversal Magnetic Field Intensity, $B_{\perp}(t)$	Resonance Condition	Complex Transverse Field, $\omega(t)$
original	$(2mc/ e \hbar)\Gamma$	$B_{\parallel} = (mc/e)\omega_0$	$\Gamma e^{i\phi_{\omega}(t)}$
generalized	$(2mc/ e \hbar)\omega_{\mathcal{H}}(t)$	$B_{\parallel}(t) = (mc/e)\dot{\phi}_{\omega}(t)$	$\Gamma \cos(\lambda t) e^{i\phi_{\omega}(t)}$
generalized	$(2mc/ e \hbar)\omega_{\mathcal{H}}(t)$	$B_{\parallel}(t) = (mc/e)\dot{\phi}_{\omega}(t)$	$\Gamma(1 + \lambda t)^{-2} e^{i\phi_{\omega}(t)}$
generalized	$(2mc/ e \hbar)\omega_{\mathcal{H}}(t)$	$B_{\parallel}(t) = (mc/e)\dot{\phi}_{\omega}(t)$	$\Gamma e^{-\lambda t} e^{i\phi_{\omega}(t)}$

TABLE II: Illustrative representation of the complex transverse field $\omega(t)$, the resonance condition in terms of the longitudinal magnetic field intensity $B_{\parallel}(t)$, and the transverse magnetic field intensity $B_{\perp}(t)$ in the selected four Rabi scenarios.

Table II summarizes the main characteristics of the four quantum mechanical evolutions that we consider in this paper. In the next section, we will use the transition probabilities in Eqs. (55) and (57) to construct our parametrized output quantum states.

IV. OPTIMUM PATHS, ENTROPIC SPEED, AND ENTROPY PRODUCTION RATE

In this section, we use the Fisher information (see Eq. (4) in Section II) to introduce a metric on a manifold of probability vectors, where the latter represents transition probabilities in each of the four quantum mechanical evolutions generated by our generalized $\text{su}(2; \mathbb{C})$ Hamiltonian models (see Eqs. (55) and (57) in Section III). By using a minimum-action principle to deduce the optimum path on this manifold between an initial source state and a final target state, we verify that this optimum path is the geodesic (shortest) path between the two points representing the states and further, this path also serves to minimize the total entropy production during the evolution. We also demonstrate by explicitly calculating the entropic speed (see Eq. (28)) and the entropy production rate (see Eq. (29) in each scenario, that to a faster transition between states there necessarily corresponds a higher rate of entropy production. For an intriguing presentation on the link between the geometry of evolving probabilities and quantum theory, we refer to Ref. [92].

A. Use of the Fisher information in physics

To motivate our analysis, we note that the Fisher information has been used to characterize the evolution of many different kinds of physical systems. It was first introduced by Fisher [93] in statistical estimation theory, and was utilized by Linnik [94] as part of an information-theoretic proof of the central limit theorem in probability theory. For this reason, the Fisher information is sometimes called the Linnik functional. However, it has also been used to prove results of the kinetic theory of gases. It was noted by McKean that the Fisher information monotonically decreases with time along solutions to Kac's model of a one-dimensional Maxwellian gas [95], and this result was later extended to gases in two-dimensional [96] and any-dimensional [97] velocity spaces by Toscani and Villani, respectively. Villani also proved the same monotonically decreasing behavior of the Fisher information along solutions to the spatially homogeneous Landau equation, again for a Maxwellian gas in any dimension of velocity space [98, 99].

Inspired by these ideas, our information geometric characterization of paths in quantum mechanical evolution focuses on the Fisher information and its behavior along solutions to a differential equation encoding the constraint of minimum entropy production.

B. Deriving probability paths from quantum evolution

Recall that in Section II (see Eq. (8)) we exploited the phase indeterminacy of state vectors in quantum mechanics to make the Fubini-Study metric tensor components $g_{\alpha\beta}^{(\text{FS})}(\theta)$ proportional to the Fisher metric tensor components $\mathcal{F}_{\alpha\beta}(\theta)$. In particular, we chose a basis of orthonormal vectors $\{|w\rangle, |w_{\perp}\rangle\}$ for the n -qubit Hilbert space \mathcal{H}_2^n such that $\text{Im}(\langle\psi|w\rangle\langle w|d\psi_{\perp}\rangle) = 0 = \text{Im}(\langle\psi|w_{\perp}\rangle\langle w_{\perp}|d\psi_{\perp}\rangle)$, which caused the non-negative variance of the phase changes to vanish in the definition of $g_{\alpha\beta}^{(\text{FS})}(\theta)$ [11, 42]. Recall also that in Section III, we derived transition probabilities $\mathcal{P}_{|w_{\perp}\rangle \rightarrow |w\rangle}(t)$ for four special cases starting from a generalized Hamiltonian for a two-level quantum system. What we now consider, building upon the connections explored between analog quantum search algorithms and two-level quantum systems [44, 45], is a set of output states $|\psi(\theta)\rangle$ of a continuous-time quantum search algorithm. Expressed

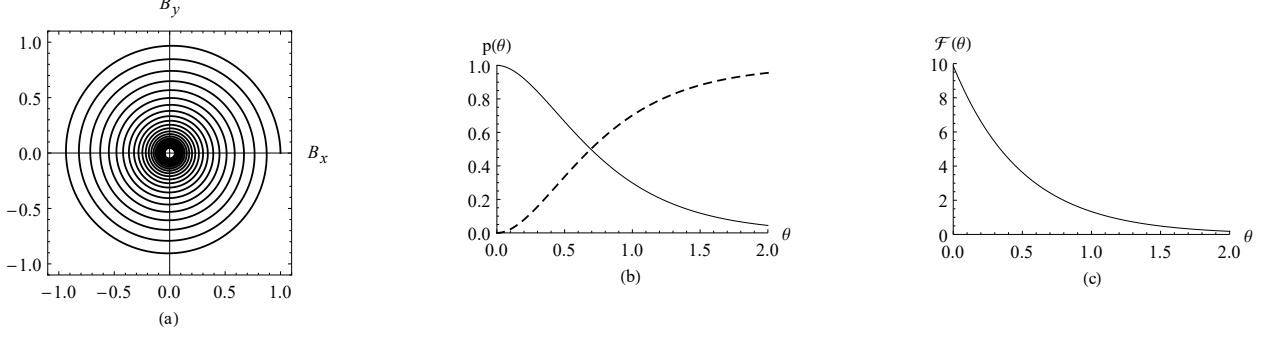


FIG. 1: In plot (c), we depict the behavior of the Fisher information $\mathcal{F}(\theta)$ versus θ . The Fisher information is defined in terms of the transition probabilities $p_w(\theta)$ (dashed line) and $p_{w_\perp}(\theta)$ (solid line) that appear in plot (b). These probabilities, in turn, arise from the particular external magnetic field $\vec{B} = \vec{B}_\perp + \vec{B}_\parallel$ with $\vec{B}_\perp = B_x \hat{x} + B_y \hat{y}$ depicted in plot (a) that specifies the $\text{su}(2; \mathbb{C})$ Hamiltonian model being studied. In plots (b) and (c), we set $\lambda = 1$ and $\Gamma/\hbar\lambda = \pi/2$ and. In plot (a), the two-dimensional parametric plot of the transverse magnetic field components, we set $\lambda = 1$ and $|\omega_0| = 15\pi$. Furthermore, for simplifying normalization purposes, we also set $\Gamma/\mu_{\text{Bohr}} = 1$ where μ_{Bohr} denotes the Bohr magneton in plot (a). All physical quantities are assumed to be conveniently expressed by means of the MKSA unit system. Finally, the $\text{su}(2; \mathbb{C})$ Hamiltonian model taken into consideration in this figure corresponds to the fourth scenario analyzed in this manuscript.

in our basis, this takes the form,

$$|\psi(\theta)\rangle \stackrel{\text{def}}{=} e^{i\varphi_w(\theta)} \sqrt{p_w(\theta)} |w\rangle + e^{i\varphi_{w_\perp}(\theta)} \sqrt{p_{w_\perp}(\theta)} |w_\perp\rangle. \quad (58)$$

We assume the input to the algorithm to be an $N = 2^n$ -dimensional normalized n -qubit source state $|s\rangle \stackrel{\text{def}}{=} |\psi(\theta_0)\rangle$, such that $|\psi(\theta)\rangle \in \mathcal{H}_2^n$ and the n -qubit Hilbert space is spanned by $\{|w\rangle, |w_\perp\rangle\}$. We interpret the parameter θ as the elapsed time t in a statistical sense. More specifically, θ represents some measurable observable varying with time that can be determined experimentally (for example, a time-varying magnetic field intensity). We note that treating elapsed time as an experimentally controllable statistical parameter is not an unusual idea. Indeed, it is not dissimilar from the idea of the Wick rotation [100], in which the inverse temperature $\beta \stackrel{\text{def}}{=} (k_B T)^{-1}$ (where $k_B \simeq 1.38 \times 10^{-23}$ [MKSA] is the Boltzmann constant) is replaced with the imaginary time it/\hbar so as to turn calculations of quantum mechanical transition amplitudes into calculations resembling statistical mechanical averages of observables. One can think of θ as the parameter along which one drives the evolution of the quantum mechanical system.

The central question can then be stated as: which paths through the space of states parametrized by θ are optimal under the constraint of minimum entropy production? We answer this question by considering the manifold of probability distributions $p(\theta)$ generated by the output states $|\psi(\theta)\rangle$ as follows,

$$|\psi(\theta)\rangle \mapsto p(\theta) = (p_w(\theta), p_{w_\perp}(\theta)) = \left(|\langle w|\psi(\theta)\rangle|^2, |\langle w_\perp|\psi(\theta)\rangle|^2 \right), \quad (59)$$

where $p_w(\theta) \stackrel{\text{def}}{=} |\langle w|\psi(\theta)\rangle|^2$ and $p_{w_\perp}(\theta) \stackrel{\text{def}}{=} |\langle w_\perp|\psi(\theta)\rangle|^2$ are the squared probability amplitudes denoting the success and failure probabilities respectively, of the analog quantum search algorithm. In our following analysis, we use the Fisher metric tensor in Eq. (4) (which, given our working assumptions, is proportional to the Fubini-Study metric in Eq. (8)), and without loss of generality, we assume the initial input state to be $|\psi(\theta_0)\rangle = |w_\perp\rangle$.

As an illustration of what follows, we show in Fig. 1 the behavior of the Fisher information evaluated along the probabilities obtained from the $\text{su}(2; \mathbb{C})$ quantum evolution with an exponentially decaying transverse field intensity, given by $\omega_{\mathcal{H}}^{(4)}(t)$ in Eq. (56).

C. Illustrative examples: Four types of driving scheme

The form of the Fisher information $\mathcal{F}(\theta)$ as a function of the driving parameter θ is fundamental to the structure of the manifold, and therefore to the behavior of the paths γ_θ with $\theta = \theta(\xi)$ (where ξ is an affine parameter) which describes the evolution.

For the sake of clarity, we point out that optimum cooling paths are Riemannian geodesic paths with respect to the dimensionless thermodynamic time t_{th} with $dt_{\text{th}} \stackrel{\text{def}}{=} d\tau'/\tau_*$ where $\tau' \in [0, \bar{\tau}]$ is the clock-time, while $\bar{\tau}$ and τ_* denotes the duration and the mean internal relaxation time of the physical process being considered, respectively. With this notation in mind, the divergence in Eq. (22) can be recast as [15, 18],

$$\mathcal{I}(\bar{\tau}) \stackrel{\text{def}}{=} \tau_* \int_0^{\bar{\tau}} \frac{d\theta^\alpha}{d\tau'} g_{\alpha\beta}(\theta) \frac{d\theta^\beta}{d\tau'} d\tau' = \int_0^{\bar{\tau}/\tau_*} \frac{d\theta^\alpha}{dt_{\text{th}}} g_{\alpha\beta}(\theta) \frac{d\theta^\beta}{dt_{\text{th}}} dt_{\text{th}}. \quad (60)$$

Upon identifying the duration of the process τ with $\bar{\tau}/\tau_*$ and the affine parameter ξ with the dimensionless thermodynamic time t_{th} , the divergence can henceforth be written as

$$\mathcal{I}(\tau) \stackrel{\text{def}}{=} \int_0^\tau \frac{d\theta^\alpha}{d\xi} g_{\alpha\beta}(\theta) \frac{d\theta^\beta}{d\xi} d\xi. \quad (61)$$

In Section III, we introduced four different schemes characterized by different functional forms of the transverse field intensity $\omega_{\mathcal{H}}(t)$ in the generalized Rabi scenario (constant, oscillatory, power-law decay, and exponential decay). The transition probabilities in each of these schemes (see Eq. (57)) will generate a corresponding functional form for the Fisher information, which in turn determines the form of the geodesic equations which describe the optimum paths. One can then compute from these optimum paths a characteristic entropic speed v_E and entropy production rate r_E that differs in each of the four cases.

1. Constant Fisher information

The first case we consider is the case of constant Fisher information, generated by a constant temporal behavior of the transverse field intensity (see Eqs. (54) and (55)). Therefore, as specified in Eqs. (58) and (59), we consider the manifold of probability distributions $\{p(\theta)\}$ with $p(\theta) \stackrel{\text{def}}{=} (p_w(\theta), p_{w\perp}(\theta))$ where the success and failure probabilities are given by,

$$p_w(\theta) \stackrel{\text{def}}{=} \sin^2\left(\frac{\Gamma}{\hbar}\theta\right), \text{ and } p_{w\perp}(\theta) \stackrel{\text{def}}{=} \cos^2\left(\frac{\Gamma}{\hbar}\theta\right), \quad (62)$$

respectively. In this case, the probabilities oscillate with a period of $T \stackrel{\text{def}}{=} \pi\hbar/\Gamma$. The Fisher information (Eq. (4)) is a constant, \mathcal{F}_0 , given by,

$$\mathcal{F}(\theta) = \mathcal{F}_0 \stackrel{\text{def}}{=} 4\left(\frac{\Gamma}{\hbar}\right)^2. \quad (63)$$

Since we are considering a single-parameter probability space, the geodesic equations in Eq. (26) simplify to,

$$\frac{d^2\theta}{d\xi^2} + \frac{1}{2\mathcal{F}} \frac{d\mathcal{F}}{d\theta} \left(\frac{d\theta}{d\xi}\right)^2 = 0. \quad (64)$$

Moreover, since $\frac{d\mathcal{F}}{d\theta} = 0$, Eq. (64) is equivalent to,

$$\frac{d^2\theta}{d\xi^2} = 0, \quad (65)$$

which, assuming initial conditions $\theta(\xi_0) = \theta_0 \in \mathbb{R}_+$ and $\dot{\theta}(\xi_0) = \dot{\theta}_0 \in \mathbb{R}_+$, yields simple optimum paths of the form,

$$\theta(\xi) = \theta_0 + \dot{\theta}_0(\xi - \xi_0). \quad (66)$$

We can now compute the entropic speed and the entropy production rate for these optimum paths. Using Eqs. (28) and (66), we find that the entropic speed v_E is given by,

$$v_E(\Gamma) = \frac{\Gamma}{\hbar} \dot{\theta}_0. \quad (67)$$

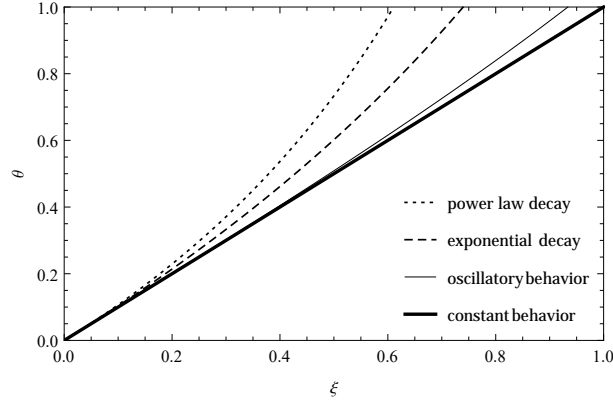


FIG. 2: Plot of the analytical expressions of the geodesic paths in the four scenarios being considered: Power law decay of the Fisher information (dotted), exponential decay of the Fisher information (dashed), oscillatory behavior of the Fisher information (thin solid), and constant behavior of the Fisher information (thick solid): In all plots, we set $\theta_0 = 0$, $\dot{\theta}_0 = 1$, $\Gamma/\hbar = 1$, and $\lambda = 2/\pi$.

Furthermore, using Eqs. (61) and (66), we find that the rate of total entropy production r_E is given by,

$$r_E(\Gamma) = \left(\frac{\Gamma}{\hbar}\right)^2 \dot{\theta}_0^2. \quad (68)$$

We remark that both the entropic speed and the entropy production rate depend on the magnitude Γ of the transverse field $\omega_{\mathcal{H}}^{(1)}(t)$, with $v_E(\Gamma) \propto \Gamma$ and $r_E(\Gamma) \propto \Gamma^2$. Therefore, one can simply manipulate the quantity Γ to find a desired trade-off between speed and entropy production rate in the quantum mechanical evolution under investigation. This is the first example of such a trade-off in our information geometric analysis.

2. Oscillatory behavior of the Fisher information

The second case we consider is the case of oscillatory Fisher information, generated by an oscillatory behavior of the transverse field intensity (see Eqs. (56) and (57)). Thus, by recalling Eqs. (58) and (59), we are led to consider the manifold of probability distributions $\{p(\theta)\}$ with $p(\theta) \stackrel{\text{def}}{=} (p_w(\theta), p_{w\perp}(\theta))$ where the success and failure probabilities are of the form,

$$p_w(\theta) \stackrel{\text{def}}{=} \sin^2 \left[\frac{\Gamma}{\hbar\lambda} \sin(\lambda\theta) \right], \text{ and } p_{w\perp}(\theta) \stackrel{\text{def}}{=} \cos^2 \left[\frac{\Gamma}{\hbar\lambda} \sin(\lambda\theta) \right], \quad (69)$$

respectively. Note that the success probabilities oscillate with a period of $T \stackrel{\text{def}}{=} \pi/\lambda$. For the sake of simplicity, we shall fix $\Gamma = (h/4)\lambda$ such that $p_w(\theta)$ reaches a maximum value of one at $\theta^* \stackrel{\text{def}}{=} \pi/(2\lambda)$. We remark that there does not need to be a strict connection between Γ and λ in order to achieve a maximum value of one. In fact, for $\Gamma \geq (h/4)\lambda$, the smallest positive θ for which $p_w(\theta)$ reaches a maximum value of one is given by $\tilde{\theta}^* \stackrel{\text{def}}{=} (1/\lambda) \sin^{-1}(\hbar\lambda/\Gamma)$. By using these expressions for $p_w(\theta)$ and $p_{w\perp}(\theta)$ to compute the Fisher information, we obtain

$$\mathcal{F}(\theta) = 4 \left(\frac{\Gamma}{\hbar}\right)^2 \cos^2(\lambda\theta). \quad (70)$$

With this expression for $\mathcal{F}(\theta)$, the geodesic equation in Eq. (64) becomes,

$$\frac{d^2\theta}{d\xi^2} - \lambda \tan(\lambda\theta) \left(\frac{d\theta}{d\xi}\right)^2 = 0. \quad (71)$$

As before, we assume initial conditions $\theta(\xi_0) = \theta_0 \in \mathbb{R}_+$ and $\dot{\theta}(\xi_0) = \dot{\theta}_0 \in \mathbb{R}_+$, and determine that Eq. (71) yields optimum paths $\theta(\xi)$ of the following general form,

$$\theta(\xi) = \theta_0 + \frac{\sqrt{1 - \lambda^2 \xi_0^2}}{\lambda} \dot{\theta}_0 [\sin^{-1}(\lambda\xi) - \sin^{-1}(\lambda\xi_0)]. \quad (72)$$

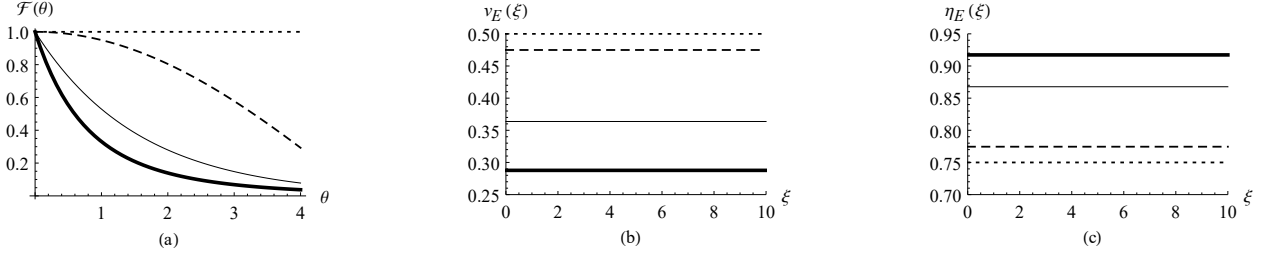


FIG. 3: In plots (a), (b), and (c), we depict the behavior of the Fisher information $\mathcal{F}(\theta)$ versus θ , the entropic speed $v_E(\xi)$ versus ξ , and the entropic efficiency $\eta_E(\xi)$ versus ξ , respectively. Dotted, dashed, thin solid, and thick solid lines in plots (a), (b), and (c) correspond to constant, oscillatory, exponential decay, and power law decay of the Fisher information, respectively. In all plots, we set $\lambda = 1/\pi$, $\Gamma/(\hbar\lambda) = \pi/2$, $\theta_0 = 1$, and $\dot{\theta}_0 = 1$. Finally, all physical quantities are assumed to be conveniently expressed by means of the MKSA unit system.

These paths specify a particular motion on the statistical manifold, with an entropic speed v_E given by,

$$v_E(\Gamma) = \frac{\Gamma}{\hbar} |\cos(\lambda\theta_0)| \dot{\theta}_0, \quad (73)$$

and a rate of entropy production r_E given by,

$$r_E(\Gamma) = \left(\frac{\Gamma}{\hbar}\right)^2 \cos^2(\lambda\theta_0) \dot{\theta}_0^2. \quad (74)$$

Compared to the first scenario (Eqs. (73) and (74)), this second scenario exhibits geodesic motion characterized by cooler paths (lower entropy production rate) traversed with slower speed (lower entropic speed).

3. Power law decay of the Fisher information

The third case we consider is the case of a power-law decay of the Fisher information, resulting from a power-law behavior of the transverse field intensity (see Eqs. (56) and (57)). Once again exploiting Eqs. (58) and (59), we consider the manifold of probability distributions $\{p(\theta)\}$ with $p(\theta) \stackrel{\text{def}}{=} (p_w(\theta), p_{w_\perp}(\theta))$ where the success and failure probabilities are defined as,

$$p_w(\theta) \stackrel{\text{def}}{=} \sin^2 \left[\frac{\Gamma}{\hbar\lambda} \left(1 - \frac{1}{1 + \lambda\theta} \right) \right], \text{ and } p_{w_\perp}(\theta) \stackrel{\text{def}}{=} \cos^2 \left[\frac{\Gamma}{\hbar\lambda} \left(1 - \frac{1}{1 + \lambda\theta} \right) \right], \quad (75)$$

respectively. Observe that when $\Gamma = (\hbar/4)\lambda$, the success probability $p_w(\theta)$ approaches one asymptotically and monotonically as θ goes to infinity. With these probabilities, the Fisher information $\mathcal{F}(\theta)$ takes the form,

$$\mathcal{F}(\theta) = 4 \left(\frac{\Gamma}{\hbar} \right)^2 \frac{1}{(1 + \lambda\theta)^4}, \quad (76)$$

which implies that the geodesic equation in Eq. (64) becomes,

$$\frac{d^2\theta}{d\xi^2} - \frac{2\lambda}{1 + \lambda\theta} \left(\frac{d\theta}{d\xi} \right)^2 = 0. \quad (77)$$

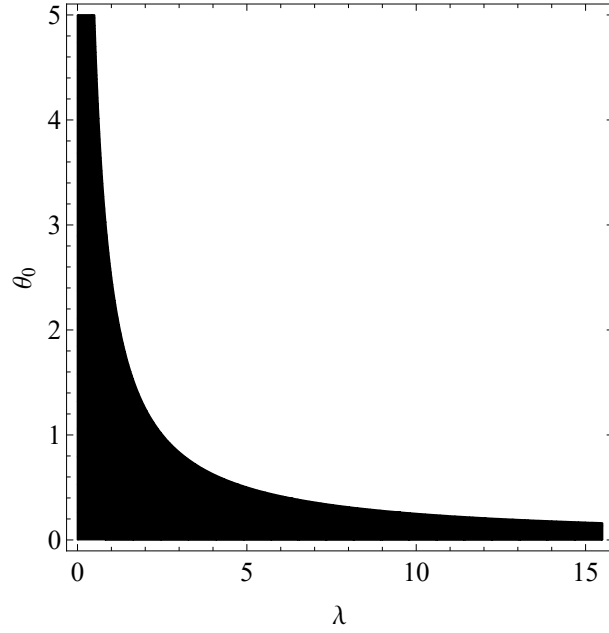


FIG. 4: Plot of the two-dimensional parametric region \mathcal{P} where the power law decay strategy is being outperformed by the exponential decay strategy in terms of higher entropic speed values. As the numerical values of λ become sufficiently large, the black region \mathcal{P} tends to vanish.

Once again assuming initial conditions $\theta(\xi_0) = \theta_0 \in \mathbb{R}_+$ and $\dot{\theta}(\xi_0) = \dot{\theta}_0 \in \mathbb{R}_+$, we obtain the following general form for the optimum paths that solve Eq. (77),

$$\theta(\xi) = \frac{(1 + \lambda\theta_0)^2 + \lambda\dot{\theta}_0 \left[(\xi - \xi_0) - \frac{1 + \lambda\theta_0}{\lambda\dot{\theta}_0} \right]}{\lambda^2 \dot{\theta}_0 \left[\frac{1 + \lambda\theta_0}{\lambda\dot{\theta}_0} - (\xi - \xi_0) \right]}. \quad (78)$$

These paths specify a motion on the statistical manifold with an entropic speed v_E given by,

$$v_E(\Gamma) = \frac{\Gamma}{\hbar} \frac{1}{[1 + \lambda(\Gamma)\theta_0]^2} \dot{\theta}_0, \quad (79)$$

and an entropy production rate r_E given by,

$$r_E(\Gamma) = \left(\frac{\Gamma}{\hbar} \right)^2 \frac{1}{[1 + \lambda(\Gamma)\theta_0]^4} \dot{\theta}_0^2. \quad (80)$$

where we define $\lambda(\Gamma) \stackrel{\text{def}}{=} (4\Gamma)/\hbar$. We find once again, comparing with the first and second scenarios, that the present scenario produces even cooler paths with even slower speed (less entropy production rate and less entropic speed).

4. Exponential decay of the Fisher information

The fourth and final case we consider is the case of exponentially decaying Fisher information, produced by an exponentially decaying magnitude of the transverse field intensity (see Eqs. (56) and (57)). Employing Eqs. (58) and (59), we analyze the manifold of probability distributions $\{p(\theta)\}$ with $p(\theta) \stackrel{\text{def}}{=} (p_w(\theta), p_{w\perp}(\theta))$ with success and failure probabilities

$$p_w(\theta) \stackrel{\text{def}}{=} \sin^2 \left[\frac{\Gamma}{\hbar\lambda} (1 - e^{-\lambda\theta}) \right], \text{ and } p_{w\perp}(\theta) \stackrel{\text{def}}{=} \cos^2 \left[\frac{\Gamma}{\hbar\lambda} (1 - e^{-\lambda\theta}) \right], \quad (81)$$

respectively. Similarly to the third scenario, letting $\Gamma = (h/4)\lambda$ causes the success probability to asymptotically and monotonically approach the ideal value of one as θ approaches infinity. The Fisher information $\mathcal{F}(\theta)$ in this case becomes,

$$\mathcal{F}(\theta) = 4 \left(\frac{\Gamma}{h} \right)^2 e^{-2\lambda\theta}, \quad (82)$$

which implies that the geodesic equation in Eq. (64) reduces to,

$$\frac{d^2\theta}{d\xi^2} - \lambda \left(\frac{d\theta}{d\xi} \right)^2 = 0. \quad (83)$$

Using the same initial conditions $\theta(\xi_0) = \theta_0 \in \mathbb{R}_+$ and $\dot{\theta}(\xi_0) = \dot{\theta}_0 \in \mathbb{R}_+$ as before, this geodesic equation yields the following general form for optimum paths,

$$\theta(\xi) = \theta_0 - \frac{1}{\lambda} \log \left[1 - \lambda \dot{\theta}_0 (\xi - \xi_0) \right]. \quad (84)$$

The motion characterized by these paths exhibits an entropic speed v_E given by,

$$v_E(\Gamma) = \frac{\Gamma}{h} e^{-\lambda(\Gamma)\theta_0} \dot{\theta}_0, \quad (85)$$

and a rate of entropy production r_E given by,

$$r_E(\Gamma) = \left(\frac{\Gamma}{h} \right)^2 e^{-2\lambda(\Gamma)\theta_0} \dot{\theta}_0^2, \quad (86)$$

where as before we have defined $\lambda(\Gamma) \stackrel{\text{def}}{=} (4\Gamma)/h$. Of the four cases we have considered, this final case exhibits the coolest optimum paths with the slowest speed (lowest entropy production rate and lowest entropic speed).

With all four cases analyzed, we plot in Fig. 2 the expressions we derived for the geodesic paths from all four cases, starting from the initial conditions $\theta_0 = 0$ and $\dot{\theta}_0 = 1$. Furthermore, we set $\Gamma/h = 1$ and $\lambda = 2/\pi$. By imposing these assumptions in Eqs. (66), (72), (78), and (84), we obtain,

$$\theta(\xi) = \xi, \quad \theta(\xi) = \frac{\pi}{2} \sin^{-1} \left(\frac{2}{\pi} \xi \right), \quad \theta(\xi) = \frac{\pi}{2} \frac{\xi}{\frac{\pi}{2} - \xi}, \quad \text{and} \quad \theta(\xi) = \frac{\pi}{2} \log \left(\frac{1}{1 - \frac{2}{\pi} \xi} \right), \quad (87)$$

for the constant case, the oscillatory case, the power-law case, and the exponential case, respectively. We also plot, in Fig. 3, the Fisher information $\mathcal{F}(\theta)$ along with the constant values of the entropic speed and entropy production rate for each of the four cases. Each new case we considered exhibited cooler optimum paths, albeit with slower entropic speed. This result is summarized by the following observation,

$$0 \leq e^{-\lambda\theta_0} \leq \frac{1}{(1 + \lambda\theta_0)^2} \leq |\cos(\lambda\theta_0)| \leq 1, \quad (88)$$

when $\theta_0 \in \mathbb{R}_+$ and $\lambda(\Gamma) \stackrel{\text{def}}{=} (4\Gamma)/h \gg 1$. However, this ranking is not true for all values of λ . In particular, when $0 \leq \lambda \lesssim 1$, we find that the entropic speed in the exponential scenario can outperform that of the power-law scenario. To quantify this statement, note that Eqs. (79) and (85) imply,

$$v_E^{(\text{power-law})}(\Gamma) = \frac{e^{\lambda\theta_0}}{(1 + \lambda\theta_0)^2} v_E^{(\text{power-law})}(\Gamma). \quad (89)$$

If we define the function $f_{\mathcal{P}}(\lambda, \theta_0)$ as,

$$f_{\mathcal{P}}(\lambda, \theta_0) \stackrel{\text{def}}{=} \frac{e^{\lambda\theta_0}}{(1 + \lambda\theta_0)^2}, \quad (90)$$

then the values of λ and θ_0 for which this function is negative correspond to values for which the exponential decay scenario gives entropic speeds that are higher than the power-law decay scenario. We formally express this as a parametric region \mathcal{P} defined as,

$$\mathcal{P} \stackrel{\text{def}}{=} \{(\lambda, \theta_0) \in \mathbb{R}_+ \times \mathbb{R}_+ : f_{\mathcal{P}}(\lambda, \theta_0) < 0\}, \quad (91)$$

Quantum Search	Hamiltonian Model	Fisher Information	Speed	Entropy Production Rate
Grover-like	original, constant B_{\perp}	constant	higher	higher
Grover-like	generalized, oscillating B_{\perp}	oscillatory	high	high
fixed-point-like	generalized, power law decay of B_{\perp}	power law decay	low	low
fixed-point-like	generalized, exponential decay of B_{\perp}	exponential decay	lower	lower

TABLE III: Illustrative representation of the entropy production rate, speed, and Fisher information in the chosen four $\text{su}(2; \mathbb{C})$ Hamiltonian models. Furthermore, for each model, we emphasize the Grover-like or fixed-point-like property possessed by its corresponding continuous time quantum search algorithm.

and plot this region in Fig. 4. It is seen clearly that sufficiently large values for λ cause the power-law strategy to perform better than the exponential strategy in terms of entropic speed. We note that a typical value of λ in experiments may be estimated by assuming a magnetic field intensity B_{\perp} of approximately 0.2 T (typical of neodymium magnets), and recalling that $\lambda = (4\Gamma)/h$ with $\Gamma = (|e|\hbar B_{\perp})/(2mc)$. This yields a value $\lambda \simeq 37$ [MKSA].

Our findings are summarized in Table III, where we describe the behavior of the Fisher information $\mathcal{F}(\theta)$, the entropic speed v_E , and the entropy production rate r_E for each of the four scenarios alongside a description of the Hamiltonian models that produce them. We also list for each case the type of continuous-time quantum search algorithm that resembles the quantum evolution.

V. CONCLUDING REMARKS

In what follows, we present a summary of main results, as well as limitations and further investigations.

A. Summary

In this paper, we presented an information geometric characterization of entropic speeds (see Eq. (28)) and entropy production rates (see Eq. (29)) that emerge from the geodesic motion (see Eq. (26)) on manifolds of parametrized quantum states (see Eq. (58)). These pure states emerge as outputs of suitable $\text{su}(2; \mathbb{C})$ time-dependent Hamiltonian evolutions (see Eq. (38)) employed to specify distinct types of continuous-time quantum search schemes. The Riemannian metrization on the manifold is specified by the Fisher information (see Eq. (4)) evaluated along the parametrized squared probability amplitudes (see Eqs. (62), (69), (75), and (81)) obtained from analysis of the quantum mechanical temporal evolution of a spin-1/2 particle in an external time-dependent magnetic field that prescribes the $\text{su}(2; \mathbb{C})$ Hamiltonian model. In Fig. 1, we show the manner in which a specific Fisher information behavior arises from a given $\text{su}(2; \mathbb{C})$ Hamiltonian model characterized by a particular magnetic field configuration (see Table II). Using a minimum action principle to transfer a quantum system from an initial state to a final state on the manifold in a finite temporal interval, we demonstrate that the minimizing (optimum) path is the shortest (geodesic, see Fig. 2) path between the two states and in particular, also minimizes the total entropy production, that is, the thermodynamic divergence of the path in Eq. (61) that occurs during the transfer (see Eqs. (26) and (27)). Then, by evaluating the entropic speed and the total entropy production along the optimum transfer paths (see Eqs. (66), (72), (78), and (84)) in the four chosen physical scenarios of interest in analog quantum search problems, we demonstrate in a clear quantitative manner that to a faster transfer there necessarily corresponds a higher entropy production rate (see Fig. 3 and Table III). We therefore conclude that lower (entropic) efficiency values do appear to accompany higher (entropic) speed values in quantum transfer processes.

In particular, the probability paths with an exponentially decaying Fisher information seem to achieve the highest entropic efficiency (see Eq. (86)) with the cost of also having the lowest entropic speed (see Eq. (85)). By contrast, the probability paths with a constant Fisher information appear to be the fastest (see Eq. (67)) but also the most inefficient from an entropic standpoint (see Eq. (68)). A graphical summary of these results, including all four $\text{su}(2; \mathbb{C})$ Hamiltonian models considered in this paper (see Table II), appear in Fig. 3, Fig. 4, and Table III.

B. Limitations and Further Investigations

In what follows, we report some limitations and insights that emerge from our information geometric analysis.

- 1) First, we focused our information geometric analysis on quantum mechanical evolutions between perfectly distinguishable initial and final quantum states. Specifically, we have assumed a vanishing quantum overlap in Eq. (45), meaning that the initial source state is exactly orthogonal to the final target state. Furthermore, we have also assumed throughout our investigation the validity of the generalized on-resonance condition as defined in Eq. (52). Clearly, we expect that scale effects and more important computational complications of transition probabilities can emerge when departing from the on-resonance condition. From a physical perspective, we also expect to find a richer dynamics where the role of essential control field is not limited to \vec{B}_\perp . For this reason we expect that \vec{B}_\parallel as well as the phase ϕ_ω will play a key role in our information geometric analysis. As pointed out by Rabi and collaborators in Ref. [78], the magnitude of \vec{B}_\perp is generally much smaller than the magnitude of \vec{B}_\parallel in a variety of nuclear resonance experiments. Interestingly, when comparing the Farhi-Gutmann analog quantum search Hamiltonian [87] with Rabi's original two-level quantum system Hamiltonian [72], the quantum overlap x between the initial and final states can be recast in terms of the magnetic field intensities B_\perp and B_\parallel [44],

$$x(B_\perp, B_\parallel) \stackrel{\text{def}}{=} \frac{B_\parallel}{B_\perp} \frac{1}{\sqrt{1 + \left(\frac{B_\parallel}{B_\perp}\right)^2}}. \quad (92)$$

Therefore, scenarios with $B_\perp \gg B_\parallel$ would correspond to cases in which $0 < x \ll 1$. Curiously, in the framework of quantum mechanical spin-1/2 particle manipulations with magnetic fields, the so-called strong-driving regime occurs when the Rabi frequency $\Omega_{\text{Rabi}} \stackrel{\text{def}}{=} \Gamma/\hbar \propto B_\perp$ is greater than the Larmor frequency $\Omega_{\text{Larmor}} \stackrel{\text{def}}{=} \Delta E/\hbar \propto B_\parallel$ with ΔE being the energy splitting between the system's states [101, 102]. In nuclear magnetic resonance experiments performed in the strong-driving regime, the intensity of the static magnetic field \vec{B}_\parallel can be less than a few micro-tesla ($B_\parallel \simeq 10^{-6}$ T, with $1 \text{ T} = 10^4 \text{ G}$) [102]. In the ultrastrong-driving regime where $B_\perp \gg B_\parallel$ for instance, the “on-resonance” driving does not appear to be a good control strategy in terms of total evolution time and/or energy-type cost functional minimization [103]. Despite the aforementioned limitations of our analysis, we truly think the information geometric approach proposed in this paper deserves further investigation since it could be leveraged to address a very important problem in quantum information processing, namely provide a theoretical basis for a first of its kind quantitative classification scheme for the various driving regimes in spin manipulations based upon both thermodynamic efficiency and minimum evolution time. In view of these arguments, it is our intention to extend our understanding of these topics by considering both departures from perfect distinguishability and generalized out-of-resonance conditions (for further details, see also Ref. [47]) in our future information geometric investigations.

- 2) Second, we emphasize that in the framework of finite-time thermodynamics, the rate of entropy production $d\sigma/dt$ (that is, r_E in our terminology) is constant along an optimum path (that is, optimal process trajectory) only for linear processes [17]. These processes are characterized by Onsager coefficients L_{ij} [104, 105] that do not depend on the fluxes \dot{X}_i , with fluxes being the rate of change in time of the particular extensive parameters X_i of the thermodynamic system (volume and internal energy, for instance). Departing from the linearity condition, it happens that [17],

$$\frac{d\sigma}{dt} + \dot{X}_i \frac{\partial R_{ij}}{\partial \dot{X}_k} \dot{X}_k \dot{X}_j = \text{constant}, \quad (93)$$

with R_{ij} being the coefficients of the so-called resistance matrix, the inverse of the matrix of Onsager coefficients L_{ij} . From Eq. (26), we note that if R_{ij} does not depend on $\dot{X} \stackrel{\text{def}}{=} dX/dt$, then the rate of entropy production $d\sigma/dt$ is constant. From an information geometric viewpoint, the relaxation of the working assumption of thermodynamic linearity would lead to a new geometrical setting where the information tensor $g_{\alpha\beta}$ would not only depend on θ but also on $\dot{\theta} \stackrel{\text{def}}{=} d\theta/d\xi$. This fact in turn, would result in a departure from the Riemannian geometric platform to what is known as a Finslerian geometric setting [106, 107]. We have not addressed the consequences of such a possible transition in our paper and it would be intriguing to investigate what would occur due to relaxation of the linearity working assumption. Interestingly, within the framework of minimum dissipation protocols in spin systems [22, 23], the components of Kirkwoods friction tensor [108] play the role of the resistance metric coefficients that appear in Eq. (93). We have limited our investigation in this paper to a single-parameter analysis with a metric tensor that does not depend on the derivative of the parameter itself. We hope to extend our analysis to multi-parameter and/or flux-dependencies in future efforts by addressing further computational challenges and gaining even deeper insights toward a realistic comparative thermodynamical

analysis of quantum search algorithms from an information geometric perspective. Finally, for a discussion on the Finslerian geometrization of Hamiltonian dynamics for physical systems with potentials depending explicitly on time and velocities, we refer to Refs. [109, 110].

- 3) Third, our work can be viewed as leading to several intriguing foundational insights. From a physics perspective, given that analog quantum search algorithms can be understood in terms of two-level quantum systems [43, 44], quantum searching can be linked to the study of the quantum mechanical evolution of an electron in an external magnetic field. From a classical electrodynamic perspective, an electric charge e moving in a magnetic field \vec{B} is deflected by a force \vec{f} proportional to the product of the charge e and velocity \vec{v} ,

$$\vec{f} = e \frac{\vec{v}}{c} \times \vec{B}. \quad (94)$$

Therefore, since the force depends upon the velocity, an electron in an external magnetic field is an example of a conservative dynamical system which is not macroscopically reversible [104, 105]. Examples of irreversible transport processes are heat conduction, electrical conduction, and *diffusion*. Interestingly, Grover's search algorithm was initially invented and presented in terms of a Markov *diffusion* process [111]. Therefore, a potentially fundamental physical insight arising from our information geometric investigation of minimum entropy product paths from quantum mechanical evolutions corresponding to two-level quantum systems mimicking analog quantum search Hamiltonian evolutions is that a realistic thermodynamic analysis of quantum search algorithms will eventually emerge from exploring the mathematical analysis of Markov processes [112, 113]. At this stage, such a statement is purely speculative. In order to provide a serious theoretical analysis of both fast and thermodynamically efficient quantum search schemes, we require a deeper understanding of the role played by fluctuations and dissipation [114, 115] in irreversible transport processes together with their connection to the physical mechanism underlying analog quantum search algorithms within realistic models of computation.

In conclusion, despite its current limitations, we view our investigation presented in this paper as a natural progression of our work presented in Refs. [42, 46]. It constitutes a nontrivial preliminary effort toward understanding quantum search algorithms from a thermodynamical perspective developed within an information geometric setting. It is our intention to improve upon the analysis provided in this paper and pursue these fascinating avenues of investigation in forthcoming scientific efforts. Of course, it is our sincere hope that our work will inspire other scientists to further explore these research avenues in the near future.

Acknowledgments

C. C. is grateful to the United States Air Force Research Laboratory (AFRL) Summer Faculty Fellowship Program for providing support for this work. Any opinions, findings and conclusions or recommendations expressed in this manuscript are those of the authors and do not necessarily reflect the views of AFRL.

-
- [1] M. R. Frey, *Quantum speed-limits-primer, perspectives, and potential future directions*, Quantum Information Processing **15**, 3919 (2016).
 - [2] D. Castelvechi, *Clash of the physical laws*, Nature **543**, 597 (2017).
 - [3] P. Faist and R. Renner, *Fundamental work cost of quantum processes*, Phys. Rev. **X8**, 021011 (2018).
 - [4] S. Campbell and S. Deffner, *Trade-off between speed and cost in shortcuts to adiabaticity*, Phys. Rev. Lett. **118**, 100601 (2017).
 - [5] W. K. Wootters, *Statistical distance and Hilbert space*, Phys. Rev. **D23**, 357 (1981).
 - [6] L. D. Landau and E. M. Lifshitz, *Statistical Physics*, Pergamon (1977).
 - [7] G. Ruppeiner, *Thermodynamics: A Riemannian geometric model*, Phys. Rev. **A20**, 1608 (1979).
 - [8] G. Ruppeiner, *Riemannian geometry in thermodynamic fluctuation theory*, Rev. Mod. Phys. **67**, 605 (1995).
 - [9] P. Salamon, J. D. Nulton, and R. S. Berry, *Length in statistical thermodynamics*, J. Chem. Phys. **82**, 2433 (1985).
 - [10] G. E. Crooks, *Measuring thermodynamic length*, Phys. Rev. Lett. **99**, 100602 (2007).
 - [11] S. L. Braunstein and C. M. Caves, *Statistical distance and geometry of quantum states*, Phys. Rev. Lett. **72**, 3439 (1994).
 - [12] T. M. Cover and J. A. Thomas, *Elements of Information Theory*, John Wiley & Sons, Inc. (2006).
 - [13] S. Amari and H. Nagaoka, *Methods of Information Geometry*, Oxford University Press (2000).
 - [14] D. Felice, C. Cafaro, and S. Mancini, *Information geometric methods for complexity*, Chaos **28**, 032101 (2018).
 - [15] P. Salamon and R. S. Berry, *Thermodynamic length and dissipated availability*, Phys. Rev. Lett. **51**, 1127 (1983).

- [16] K. H. Hoffmann, B. Andresen, and P. Salamon, *Measures of dissipation*, Phys. Rev. **A39**, 3618 (1989).
- [17] W. Spirtkl and H. Ries, *Optimal finite-time endoreversible processes*, Phys. Rev. **E52**, 3485 (1995).
- [18] L. Diosi, K. Kulacsy, B. Lukacs, and A. Racz, *Thermodynamic length, time, speed, and optimum path to minimize entropy production*, J. Chem. Phys. **105**, 11220 (1996).
- [19] L. Diosi and P. Salamon, *From statistical distances to minimally dissipative processes*, in Thermodynamics of Energy Conversion and Transport, edited by S. Sieniutycz and A. De Vos (Springer, New York, 2000), pp. 286-318.
- [20] D. A. Sivak and G. E. Crooks, *Thermodynamic metrics and optimal paths*, Phys. Rev. Lett. **108**, 190602 (2012).
- [21] D. A. Sivak and G. E. Crooks, *Near-equilibrium measurements of nonequilibrium free energy*, Phys. Rev. Lett. **108**, 150601 (2012).
- [22] G. M. Rostskoff and G. E. Crooks, *Optimal control in nonequilibrium systems: Dynamic Riemannian geometry of the Ising model*, Phys. Rev. **E92**, 060102(R) (2015).
- [23] G. M. Rostskoff, G. E. Crooks, and E. Vanden-Eijnden, *Geometric approach to optimal nonequilibrium control: Minimizing dissipation in nanomagnetic spin systems*, Phys. Rev. **E95**, 012148 (2017).
- [24] E. T. Jaynes, *Information theory and statistical mechanics. I*, Phys. Rev. **106**, 620 (1957).
- [25] E. T. Jaynes, *Information theory and statistical mechanics. II*, Phys. Rev. **108**, 171 (1957).
- [26] B. R. Frieden, *Physics from Fisher Information*, Cambridge University Press (1998).
- [27] B. R. Frieden, A. Plastino, A. R. Plastino, and B. H. Soffer, *Fisher-based thermodynamics: Its Legendre transform and concavity properties*, Phys. Rev. **E60**, 48 (1999).
- [28] B. R. Frieden, A. Plastino, A. R. Plastino, and B. H. Soffer, *Schrödinger link between nonequilibrium thermodynamics and Fisher information*, Phys. Rev. **E66**, 046128 (2002).
- [29] L. K. Grover, *Quantum mechanics helps in searching for a needle in a haystack*, Phys. Rev. Lett. **79**, 325 (1997).
- [30] M. A. Nielsen and I. L. Chuang, *Quantum Computation and Information*, Cambridge University Press (2000).
- [31] J. J. Alvarez and C. Gomez, *A comment on Fisher information and quantum algorithms*, arXiv:quant-ph/9910115 (2000).
- [32] A. Miyake and M. Wadati, *Geometric strategy for the optimal quantum search*, Phys. Rev. **A64**, 042317 (2001).
- [33] C. Cafaro and S. Mancini, *An information geometric viewpoint of algorithms in quantum computing*, AIP Conf. Proc. **1443**, 374 (2012).
- [34] C. Cafaro and S. Mancini, *On Grover's search algorithm from a quantum information geometry viewpoint*, Physica **A391**, 1610 (2012).
- [35] C. Cafaro, *Geometric algebra and information geometry for quantum computational software*, Physica **A470**, 154 (2017).
- [36] C. H. Bennett, *The thermodynamics of computation- A review*, Int. J. Theor. Phys. **21**, 905 (1982).
- [37] J. M. R. Parrondo, J. M. Horowitz, and T. Sagawa, *Thermodynamics of information*, Nat. Phys. **11**, 131 (2015).
- [38] C. Cafaro and P. van Loock, *Towards an entropic analysis of quantum error correction with imperfections*, in Bayesian Inference and Maximum Entropy Methods in Science and Engineering, AIP Conf. Proc. **1553**, 275 (2013).
- [39] C. Cafaro and P. van Loock, *An entropic analysis of approximate quantum error correction*, Physica **A404**, 34 (2014).
- [40] R. Beals, S. Brierley, O. Gray, A. W. Harrow, S. Kutin, N. Linden, D. Shepherd, and M. Stather, *Efficient distributed quantum computing*, Proc. R. Soc. **A469**, 20120686 (2013).
- [41] R. Perlmutter and Y.-K. Liu, *Thermodynamic analysis of classical and quantum search algorithms*, arXiv:quant-ph/1709.10510 (2017).
- [42] C. Cafaro and P. M. Alsing, *Decrease of Fisher information and the information geometry of evolution equations for quantum mechanical probability amplitudes*, Phys. Rev. **E97**, 042110 (2018).
- [43] T. Byrnes, G. Forster, and L. Tessler, *Generalized Grover's algorithm for multiple phase inversion states*, Phys. Rev. Lett. **120**, 060501 (2018).
- [44] C. Cafaro and P. M. Alsing, *Continuous-time quantum search and time-dependent two-level quantum systems*, Int. J. Quantum Information **17**, 1950025 (2019).
- [45] C. Cafaro and P. M. Alsing, *Theoretical analysis of a nearly optimal analog quantum search*, Physica Scripta **94**, 085103 (2019).
- [46] C. Cafaro and P. M. Alsing, *Information geometry aspects of minimum entropy production paths from quantum mechanical evolutions*, Physical Review **E101**, 022110 (2020).
- [47] C. Cafaro, S. Gassner, and P. M. Alsing, *Information geometric perspective on off-resonance effects in driven two-level quantum systems*, Quantum Reports **2**, 166 (2020).
- [48] S. Gassner, C. Cafaro, and S. Capozziello, *Transition probabilities in generalized quantum search Hamiltonian evolutions*, Int. Journal of Geometric Methods in Modern Physics **17**, 2050006 (2020).
- [49] S. L. Braunstein, C. M. Caves, and G. J. Milburn, *Generalized uncertainty relations: theory, examples, and Lorentz invariance*, Annals of Physics **247**, 135 (1996).
- [50] G. E. Crooks, *Fisher information and statistical mechanics*, Technical Note 008v4, available at <http://threeplusone.com/sher> (2012).
- [51] S. Luo, *Wigner-Yanase skew information and uncertainty relations*, Phys. Rev. Lett. **91**, 180403 (2003).
- [52] S.-L. Luo, *Fisher information of wavefunctions: Classical and quantum*, Chin. Phys. Lett. **23**, 3127 (2006).
- [53] S. Boixo, S. T. Flammia, C. M. Caves, and J. M. Geremia, *Generalized limits for single parameter quantum estimation*, Phys. Rev. Lett. **98**, 090401 (2007).
- [54] M. M. Taddei, B. M. Escher, L. Davidovich, and R. L. de Matos Filho, *Quantum speed limit for physical processes*, Phys. Rev. Lett. **110**, 050402 (2013).
- [55] D. Paiva Pires, M. Cianciaruso, L. C. Celeri, G. Adesso, and D. O. Soares-Pinto, *Generalized geometric quantum speed limits*, Phys. Rev. **X6**, 021031 (2016).

- [56] D. J. C. Bures, *An extension of Kakutani's theorem on infinite product measures to the tensor product of semifinite w^* -algebras*, Trans. Am. Math. Soc. **135**, 199 (1969).
- [57] A. Uhlmann, *The transition probability in the state space of a $*$ -algebra*, Rep. Math. Phys. **9**, 273 (1976).
- [58] C. Cafaro and S. A. Ali, *Maximum caliber inference and the stochastic Ising model*, Phys. Rev. **E94**, 052145 (2016).
- [59] P. Zanardi, L. Campos Venuti, and P. Giorda, *Bures metric over thermal state manifolds and quantum criticality*, Phys. Rev. **A76**, 062318 (2007).
- [60] A. Caticha, *Entropic Inference and the Foundations of Physics*; USP Press: São Paulo, Brazil (2012); Available online: <http://www.albany.edu/physics/ACaticha-EIFP-book.pdf>.
- [61] F. Weinhold, *Metric geometry of equilibrium thermodynamics*, J. Chem. Phys. **63**, 2479 (1975).
- [62] P. Salamon, J. Nulton, and E. Ihrig, *On the relation between entropy and energy versions of thermodynamic length*, J. Chem. Phys. **80**, 436 (1984).
- [63] F. De Felice and J. S. Clarke, *Relativity on curved manifolds*, Cambridge University Press (1990).
- [64] P. Salamon, J. D. Nulton, J. R. Harland, J. Pedersen, G. Ruppeiner, and L. Liao, *Simulated annealing with constant thermodynamic speed*, Computer Physics Communications **49**, 423 (1988).
- [65] B. Andresen and J. M. Gordon, *Constant thermodynamic speed for minimizing entropy production in thermodynamic processes and simulated annealing*, Phys. Rev. **E50**, 4346 (1994).
- [66] L. Pezzé and A. Smerzi, *Entanglement, nonlinear dynamics, and the Heisenberg limit*, Phys. Rev. Lett. **102**, 100401 (2009).
- [67] E. P. Gyftopoulos and G. P. Beretta, *Thermodynamics: Foundations and Applications*, Dover Publications, Inc. (2005).
- [68] P. Salamon, A. Nitzan, B. Andresen, and R. S. Berry, *Minimum entropy production and the optimization of heat engines*, Phys. Rev. **A21**, 2115 (1980).
- [69] N. Shiraishi, K. Saito, and H. Tasaki, *Universal trade-off relation between power and efficiency for heat engines*, Phys. Rev. Lett. **117**, 190601 (2016).
- [70] P. Pietzonka and U. Seifert, *Universal trade-off between power, efficiency, and constancy in steady-state heat engines*, Phys. Rev. Lett. **120**, 190602 (2018).
- [71] J. Anandan and Y. Aharonov, *Geometry of quantum evolution*, Phys. Rev. Lett. **65**, 1697 (1990).
- [72] J. J. Sakurai, *Modern Quantum Mechanics*, Addison-Wesley Publishing Company, Inc. (1994).
- [73] C. Cafaro and S. Mancini, *Quantum stabilizer codes for correlated and asymmetric depolarizing errors*, Phys. Rev. **A82**, 012306 (2010).
- [74] C. Cafaro and P. van Loock, *Approximate quantum error correction for generalized amplitude-damping errors*, Phys. Rev. **A89**, 022316 (2014).
- [75] L. D. Landau, *A theory of energy transfer. II*, Phys. Z. Sowjet. **2**, 46 (1932).
- [76] C. Zener, *Non-adiabatic crossing of energy levels*, Proc. R. Soc. London, Ser. **A137**, 696 (1932).
- [77] I. I. Rabi, *Space quantization in a gyrating magnetic field*, Phys. Rev. **51**, 652 (1937).
- [78] I. I. Rabi, N. F. Ramsey, and J. Schwinger, *Use of rotating coordinates in magnetic resonance problems*, Rev. Mod. Phys. **26**, 167 (1954).
- [79] N. Rosen and C. Zener, *Double Stern-Gerlach experiment and related collision phenomena*, Phys. Rev. **40**, 502 (1932).
- [80] E. Barnes and S. Das Sarma, *Analytically solvable driven time-dependent two-level quantum systems*, Phys. Rev. Lett. **109**, 060401 (2012).
- [81] A. Messina and H. Nakazato, *Analytically solvable Hamiltonians for quantum two-level systems and their dynamics*, J. Phys. A: Math. Theor. **47**, 445302 (2014).
- [82] R. Grimaudo, A. S. M. de Castro, H. Nakazato, and A. Messina, *Classes of exactly solvable generalized semi-classical Rabi systems*, Ann. Phys. (Berlin) **2018**, 1800198.
- [83] F. Bloch, *Nuclear induction*, Phys. Rev. **70**, 460 (1946).
- [84] F. Bloch, W. W. Hansen, and M. Packard, *The nuclear induction experiment*, Phys. Rev. **70**, 474 (1946).
- [85] R. K. Wangness and F. Bloch, *The dynamical theory of nuclear induction*, Phys. Rev. **89**, 728 (1953).
- [86] L. K. Grover, *Fixed-point quantum search*, Phys. Rev. Lett. **95**, 150501 (2005).
- [87] E. Farhi and S. Gutmann, *An analog analogue of a digital quantum computation*, Phys. Rev. **A57**, 2403 (1998).
- [88] A. M. Dalzell, T. J. Yoder, and I. L. Chuang, *Fixed-point adiabatic quantum search*, Phys. Rev. **A95**, 012311 (2017).
- [89] J. Bae and Y. Kwon, *Generalized quantum search Hamiltonians*, Phys. Rev. **A66**, 012314 (2002).
- [90] J. Roland and N. J. Cerf, *Quantum search by local adiabatic evolution*, Phys. Rev. **A65**, 042308 (2002).
- [91] A. Perez and A. Romanelli, *Nonadiabatic quantum search algorithms*, Phys. Rev. **A76**, 052318 (2007).
- [92] M. Reginatto and M. J. W. Hall, *Quantum theory from the geometry of evolving probabilities*, AIP Conf. Proc. **1443**, 96 (2012).
- [93] R. A. Fisher, *Theory of statistical estimation*, Proc. Cambridge Philos. Soc. **22**, 700 (1925).
- [94] Y. V. Linnik, *An information-theoretic proof of the central limit theorem with the Lindeberg condition*, Theory Probab. Appl. **4**, 288 (1959).
- [95] H. P. McKean Jr., *Speed of approach to equilibrium for Kac's caricature of a Maxwellian gas*, Arch. Rational Mech. Anal. **21**, 343 (1966).
- [96] G. Toscani, *New a priori estimates for the spatially homogeneous Boltzmann equation*, Continuum Mech. Thermodyn. **4**, 81 (1992).
- [97] C. Villani, *Fisher information estimates for Boltzmann's collision operator*, J. Math. Pures Appl. **77**, 821 (1998).
- [98] C. Villani, *On the spatially homogeneous Landau equation for Maxwellian molecules*, Math. Models Methods Appl. Sci. **8**, 957 (1998).

- [99] C. Villani, *Decrease of the Fisher information for the Landau equation with Maxwellian molecules*, Math. Models Methods Appl. Sci. **10**, 153 (2000).
- [100] G. C. Wick, *Properties of Bethe-Salpeter wave functions*, Phys. Rev. **96**, 1124 (1954).
- [101] P. London, P. Balasubramanian, B. Naydenov, L. O. McGuinness, and F. Jelezko, *Strong driving of a single spin using arbitrarily polarized fields*, Phys. Rev. **A90**, 012302 (2014).
- [102] J. H. Shim, S.-J. Lee, K.-K. Yu, S.-M. Hwang, and K. Kim, *Strong pulsed excitations using circularly polarized fields for ultra-low field NMR*, J. Mag. Res. **239**, 87 (2014).
- [103] M. Hirose and P. Cappellaro, *Time-optimal control with finite bandwidth*, Quantum information Processing **17**, 88 (2018).
- [104] L. Onsager, *Reciprocal relations in irreversible processes. I*, Phys. Rev. **37**, 405 (1931).
- [105] L. Onsager, *Reciprocal relations in irreversible processes. II*, Phys. Rev. **38**, 2265 (1931).
- [106] M. Di Bari and P. Cipriani, *Geometry and chaos on Riemannian and Finsler manifolds*, Planetary and Space Science **46**, 1543 (1998).
- [107] J. D. Clayton, *On Finsler geometry and applications in mechanics: Review and new perspectives*, Adv. Math. Phys. Vol. 2015, Article ID 828475, 11 pages (2015).
- [108] J. G. Kirkwood, *The statistical mechanical theory of transport processes*, J. Chem. Phys. **14**, 180 (1946).
- [109] M. Di Bari, D. Boccaletti, P. Cipriani, and G. Pucacco, *Dynamical behavior of Lagrangian systems on Finsler manifolds*, Phys. Rev. **E55**, 6448 (1997).
- [110] M. Pettini, *Geometry and Topology in Hamiltonian Dynamics and Statistical Mechanics*, Springer (2007).
- [111] L. K. Grover, *From Schrödinger's equation to the quantum search algorithm*, Am. J. Phys. **69**, 769 (2001).
- [112] J. Schnakengerg, *Network theory of microscopic and macroscopic behavior of master equation systems*, Rev. Mod. Phys. **48**, 571 (1976).
- [113] H. Ge and H. Qian, *Physical origin of entropy production, free energy dissipation, and their mathematical representations*, Phys. Rev. **E81**, 051133 (2010).
- [114] U. Marini Bettolo Marconi, A. Puglisi, L. Rondoni, and A. Vulpiani, *Fluctuation-dissipation: Response theory in statistical physics*, Phys. Rep. **461**, 111 (2008).
- [115] M. Esposito and C. Van den Broeck, *Three detailed fluctuation theorems*, Phys. Rev. Lett. **104**, 090601 (2010).